Marina Asuero Von Munthe Af Morgenstierne

Experimental measurement of airflow distribution in operating rooms

Master's thesis in Sustainable Energy - Energy use in buildings
Supervisor: Guangyu Cao
Co-supervisor: Tomas Fecer

June 2023

Master's thesis

NTNU

Norwegian University of
Science and Technology

Marina Asuero Von Munthe Af Morgenstierne

Experimental measurement of airflow distribution in operating rooms

Master's thesis in Sustainable Energy - Energy use in buildings
Supervisor: Guangyu Cao
Co-supervisor: Tomas Fecer
June 2023

Norwegian University of Science and Technology
Faculty of Engineering
Department of Energy and Process Engineering

NTNU
Norwegian University of
Science and Technology

Acknowledgments

This project was written under the guidance of Guangyu Cao and Tomáš Fečer at the Department of Energy and Process Engineering at the Norwegian University of Science and Technology.

I would like to foremost express my gratitude to my supervisor Tomáš Fečer for contributing so much to this project and being there when I needed advice and support. This study would not have been the same without your input and knowledge.

I am thankful to my supervisor Guangyu Cao for guiding me through weekly meetings, providing me with literature reviews, and taking the time to answer all my inquiries whilst sharing his knowledge on the topic.

A debt of gratitude is owed to Liv-Inger and the staff at St. Olav's Hospital for making my stay so comfortable and granting me the possibility to make two of their operating rooms study cases.

A special thank you to Dominika Kwiecińska for helping me with the mock-up surgeries and for letting me take my measurements while performing her study.

A big thank you to my friends Victoria and Denisse for morally supporting me throughout this semester and making it unforgettable.

And finally, my partner Jason, thank you for bearing with me and supporting me throughout this whole journey, your patience and understanding are very much appreciated.

Abstract

Studies show that ventilation systems take an important role to reduce surgical site infection in hospitals. However, the ventilation system itself might not be enough. Staff's movement around the room, positioning of the surgical lamps, and even the clothing worn by the surgeons can interfere with the airflow, spreading contaminating particles around the operating room. These bacteria-carrying particles emitted by personnel can be transported through thermal plumes (TP) that have the ability to influence the distribution of air in the microenvironment area of the operating room.

The objective of this study is to characterise the thermal plume of a patient under two examined ventilation systems, laminar airflow (LAF) and turbulent mixed ventilation (MV) with a variable room temperature of 21 and 23 °C. Two operating rooms (ORs) at St. Olavs Hospital were used as study cases to compare the patient's thermal plumes. During the measurements, room temperature, relative humidity, velocity, temperature, and turbulence intensity of the thermal plume were determined. As well as the experimental collection of data, theoretical calculations of the thermal plume and air distribution in the OR were assessed to understand the phenomenon and provide a thorough explanation in the discussion section.

The results show that most Indoor Air Quality (IAQ) parameters are within European standards except for the low humidity. Regarding the measurement data, the risk of SSI increases at 23 °C rather than at 21 °C for both ventilation systems. This is due to increased turbulence intensity and a reduction in the thermal plume's velocity for the MV and for LAF, the thermal plume is suppressed at 5 cm at 21 °C while reaching a height of 10 cm at 23 °C.

This master thesis is a continuation of the specialisation project submitted in December 2022 that found that thermal plumes had an important role in dominating the airflow in the critical zone and thus, having the potential to

prevent SSI.

Contents

List of Tables

LIST OF TABLES

List of Figures

List of Symbols

Acronym

ACH Air change per Hour

ADI Approximate Distributions Integration

AHU Air handling unit

BCP Bacteria-carrying particles

CFD Computational fluid dynamics

CFU Colony formation unit

EPT Eulerian particle tracking

$HVAC$ Heating, Ventilation, and Air Conditioning

IAQ Indoor air quality

LAF Laminar Airflow

LPT Lagrangian particle tracking

MV Turbulent mixed airflow

OR Operating room

PIV Particle image velocimetry

RH Relative Humidity

RT Room temperature

SSI Surgical site infections

$TCAF$ Temperature controlled airflow

TP Thermal plume

Nomenclature

β Thermal expansion coefficient

Δh Distance from heat source to ceiling

ΔS Elementary area of the plume cross section

ΔT_m Maximum air temperature excess

Γ_φ Effective diffusion coefficient

μ Molecular viscosity

$\overline{V}$ Mean velocity

Φ_h Convective heat flux

ψ Normally distributed random number

ρ Air density

ρ_p Density of particle

ρ_r Air density in the room

ρ_s Supply air density to the room

ε Dissipation rate

ε_p Particle eddy diffusivity

φ Transported quantity

$\vec{V}$ Velocity vector

A_s Area of room surfaces

C_d Drag coefficient

c_p Specific heat of air

C_x Empirical coefficient

d Heat source diameter

D_p Brownian diffusivity of particle

d_p Particle diameter

e Kinetic energy flux

E_r Kinetic energy of the room

F_B Brownian force

F_b Buoyancy force

F_D Drag force

F_s Saffman's lift term

F_{therm} Thermophoretic term

g Gravitational acceleration

H Height of the room

h Convective heat transfer coefficient

h_o Distance from virtual origin to top of heat source

I Momentum flux

k Turbulence kinetic energy

M Molecule mass

P Buoyancy force density

P Pressure

Q Enthalpy flux

q Volume flow rate

q_f Heat flux

q_s Supply volume flow rate

R Gas law constant

r Radius

R_0 Mean width of cross-section of thermal plume

$R_{t\alpha}$ Temperature local angular width

$R_{v\alpha}$ Velocity local angular width

Re_p Reynolds number

S_φ Source term

SD Standard deviation

T Temperature

t Time

t_f Fluid characteristic temperature

t_s Solid wall temperature

TI Turbulence intensity

u' Fluctuating velocity

u^* Friction velocity

u_o Mean air speed

u_r Room average velocity

LIST OF SYMBOLS

V Volume flux

v_d Particle deposition velocity

v_g Kinetic air viscosity

v_i Air velocity

v_m Maximum vertical air velocity

V_r Room volume

v_s Particle settling velocity

x Distance between wall and cell centre

LIST OF SYMBOLS

Chapter 1

Introduction

Clean air in operation rooms (ORs) is known to prevent surgical site infections (SSI) [1], which refer to the infection at the skin, tissue, or organ level within 30 to 90 days of surgery [2]. This is one of the main complications after surgery and it is also affiliated with mortality [3]. In the United States of America, SSI comes second as the most common infection, extending hospitalisation by more than a week [4]. Studies have shown that the main source of airborne bacteria is particle shedding from the surgical team and from outdoor air that enters when doors are open [5]. Air currents and human movement in the surgical room can relocate the squames and bacteria-carrying particles (BCPs) towards the sterilised area [6], [7]. Thus, a proper ventilation system is critical for an appropriate indoor environment in ORs and the well-being of patients and staff. Two systems are included in the scope of this study, laminar airflow (LAF) and turbulent mixed ventilation (MV). Previous studies have highlighted the importance of using different ventilation systems for particular surgeries. General surgeries like abdominal surgery should be performed in MV rooms while for procedures with higher infection risk such as organ transplantation, cardiovascular surgery, or surgery with a prosthetic implant, the recommendation is to use LAF ORs [8].

A previous investigation from the specialisation project showed that the

particle presence correlated to the turbulence intensity found at 10 cm above the wound, implying the existence and magnitude of the thermal plume (TP). Studies have demonstrated that BCPs can be spread around the surgical area due to thermal plumes and contaminate the surgical site [9]. Thermal plumes are an energy exchange between the body and its surroundings, causing the air to rise slowly and transporting pollutants with less density than the supply air [10]. Understanding the thermal flow is critical to recognise the airflow pattern in a room and thus the risk of SSI [11].

1.1 Objective and scope of the study

The objective of this study was to understand how different room temperatures influence the patient's thermal plume. A complementary aim was to figure out which ventilation system and under which room temperature can be more beneficial for the prevention of surgical site infections in patients based on their thermal plume.

The aim was achieved by using two operating rooms at St. Olavs Hospital as study cases, laminar airflow, and mixing ventilation. Two measurements with different room temperatures were performed with each system, 21 °C and 23 °C. During the measurements, room temperature, relative humidity, velocity, temperature, and turbulence intensity of the thermal plume were determined.

The following points were conducted to reach the finalisation of the study:

- Look into the literature review regarding different ventilation solutions, the impact of thermal plumes in surgical critical zones, and the parameter requisites in ORs.

- Understand the theoretical equations that define the plume's behavior and particle movement around the room.

- Conduct experimental measurements of the patients' thermal plume in both ORs under different room temperatures, 21 and 23 °C.

- Analyse the results to determine the effect of the thermal plume and provide a conclusion.

Chapter 2

Literature Review

Ventilation systems in operating rooms can assist in the reduction of surgical site infections and the prevention of death rates. The difference between ventilation systems currently used in hospitals is discussed as well as highlighting diverse pathways in which bacteria can be introduced into the surgical room. Literature about how thermal plumes behave in an operating room and the indoor environment conditions that they should have are also presented in this section.

2.1 Ventilation systems

Different technologies are being studied and used in hospitals to improve patients' recovery chances and reduce infection risks. Depending on the surgery, some types of ventilation systems are preferred over others [12].

2.1.1 Turbulent mixed ventilation

Under an MV ventilation system, the air is supplied from the ceiling into the room at a specific rate with the objective to generate turbulence in the room and aim to achieve a fully mixed room that promotes uniform temperatures and the dilution of the concentration of particles.

2.1.2 Laminar airflow ventilation

This system became popular in the 1960s and '70s to reduce post-operative wound infection. At the same time, antibiotics were also introduced, and thus, the effectiveness of the ventilation system was put into question [13]. Laminar airflow administers a homogeneous and unidirectional flow of air from the ceiling into the critical zone with little turbulence to avoid the creation of currents and turbulence that could contribute to the spreading of bacteria-carrying particles around the room. It uses a sweeping action to wash off the bacteria before the clean air mixes with the surrounding contaminated one.

2.1.3 Hybrid ventilation

This technology utilises both aforementioned ventilations to obtain optimal cleanness efficiency during surgeries. The unidirectional flow is used for the critical zone and the periphery of the OR is ventilated with MV.

2.1.4 Temperature controlled airflow

This modern technology uses air density differences to protect critical areas. Air is introduced into the room through LAF and due to being slightly colder, ergo heavier, than the surrounding air, it flows downwards to the operating table. A heating system located by the periphery warms up the room air, creating the density difference and ensuring the effectiveness of the vertical column over the patient. Figure 2.1 illustrates the four different ventilation systems.

2.1.5 Comparison between LAF and MV

LAF and MV are often compared in terms of airflow supply, energy consumption, and air cleanness efficiency (transportation of bacteria to the microenvironment zone). LAF requires up to 82% higher airflow supply than MV [15], and the air velocity close to the wound is twice the amount in LAF than in MV [16]. Consequently, the electricity consumption increases for LAF. A
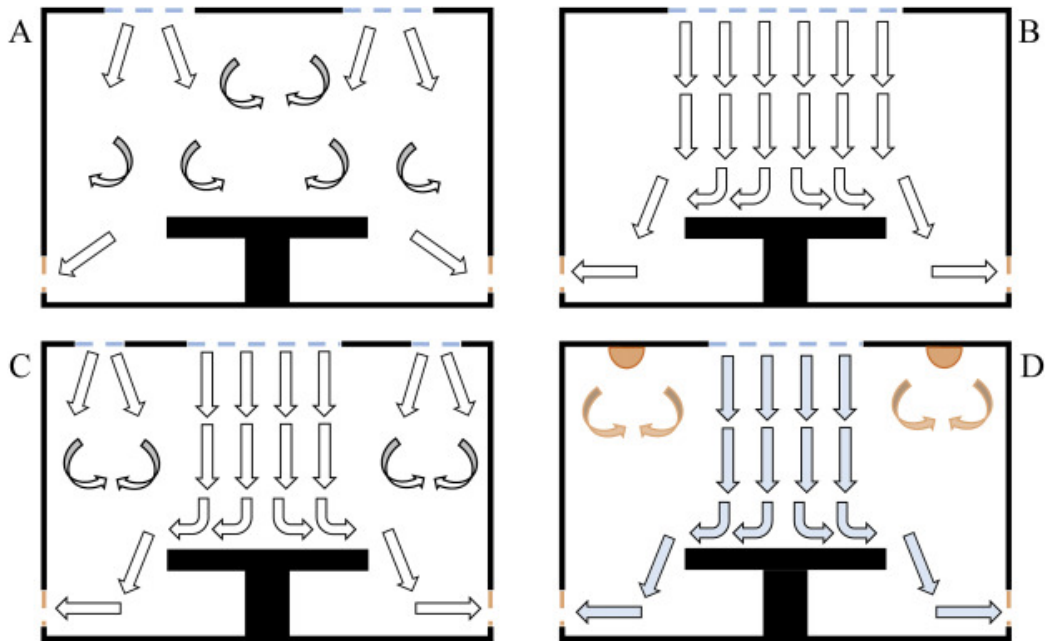
Figure 2.1: Virtual representation of different HVAC systems used in hospitals. A) Turbulent mixed ventilation (MV); B) Laminar airflow (LAF); C) Hybrid ventilation; D) Temperature controlled airflow (TCAF) [14].

study by NTNU shows that LAF increases 50 % of the MV consumption [17]. The filters and ventilation systems used for MV are simpler and require less maintenance than LAF, Making the MV a more economically friendly ventilation alternative than LAF [18], [19].

With regard to the bacterial load removal, a study done by the University of Gothenburg found that the laminar airflow system resulted in a reduction of 89% in CFU in comparison with the MV system [20]. Other studies done by the University of Lund, Sweden, have also found that LAF has significantly lower CFU than mixed ventilation [5]. Furthermore, a study by the Medical University of Vienna, states that there was no significant difference between a small LAF system (380 cm × 120 cm) and no LAF in terms of CFU counts measured and that only the large LAF system (518 cm × 380 cm) provided enough airflow to reduce the bacteria load in the critical zone [21]. However, epidemiological registry studies have shown that the risk of surgical site infections in laminar surgeries appears to be the same or higher than in MV.

For this reason, WHO has stated that laminar flow should not be used for total arthroplasty surgery [22].

The air cleanness efficiency in a room is not only related to the ventilation system but also the layout of the room and its equipment. Studies show that both solutions are susceptible to the layout of the OR such as the position of the operating table and surgical lamps and personnel movement [23]. Although the consequences of SSI are studied to be more serious under a unidirectional flow than turbulent ventilation since it can disrupt air displacement [12].

2.2 Thermal plume

The human body is continuously exchanging heat with its surrounding air and since the human body's temperature is around 36 °C, higher than the thermal comfortable air temperature, this creates a directional flow [24]. This flow is also known as a thermal plume and due to the buoyancy effect, it begins at the feet moving up close to the body until it separates at the shoulder and head level [25]. This effect can be seen in Figure 2.2a where the thermal plume begins around the hips level and makes its way close to the body until it separates at the head.

(a) Temperature contour (b) Velocity vectors
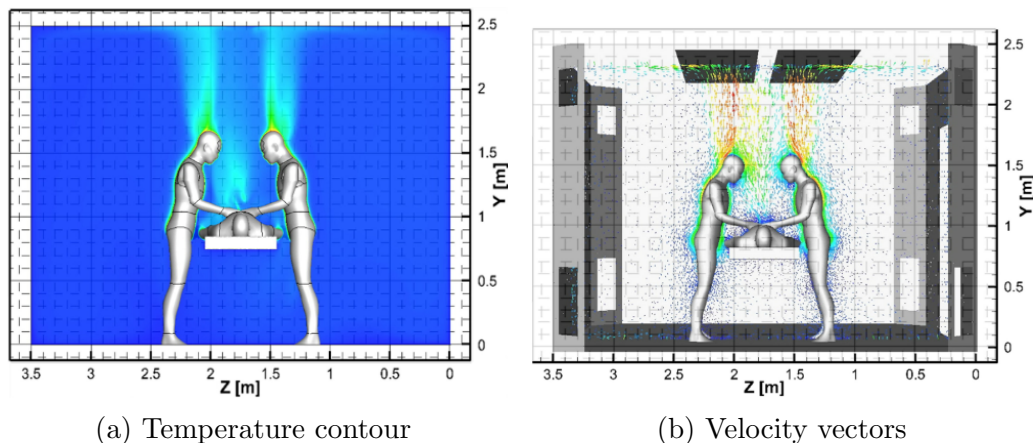
Figure 2.2: Thermal plume of a standing surgeons during surgery [26].

Unlike the strong thermal plume observed in the standing position, Fig-

ure 2.3a presents the thermal plume of a lying patient which is generated from two different areas, the core and the head. From the thermal figures, it should be noted that the thermal plume of the surgeons reaches a higher height than that of the patient.

(a) Temperature contour
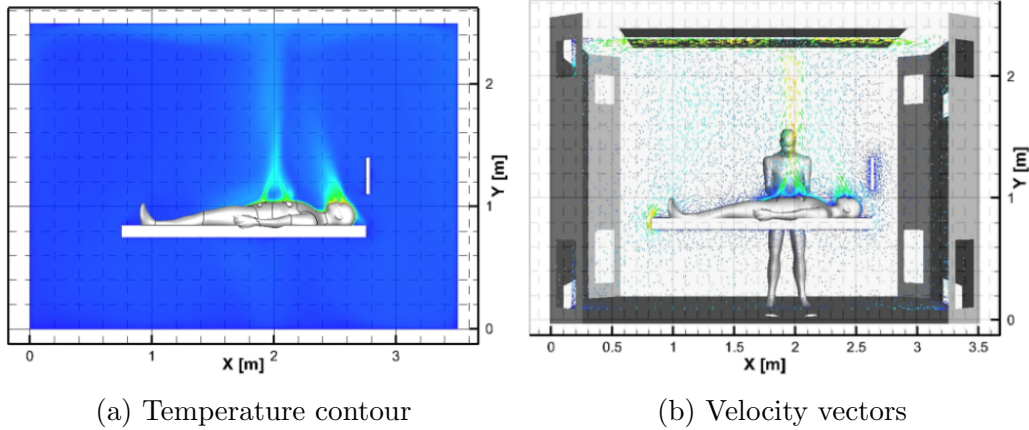
(b) Velocity vectors

Figure 2.3: Thermal plume of a lying patient during surgery [26].

Looking into the velocity vectors, Figure 2.2b and Figure 2.3b, one can observe that the plume's velocity is higher for the standing than lying position, along with showing that the higher velocity is reached in both scenarios once the plume has detached from the body. In Figure 2.3a the thermal plume located by the head has a slight angle towards the core, which it is caused by the breathing airflow.

2.3 Bacteria in ORs

It is hard to predict the size and amount of bacteria found during surgery since it is influenced by several factors. Nonetheless, a study has ascertained that under average activity, surgeons release around 10^4 particles per minute and that 10 % of these are bacterial [27]. Studies have determined that bacteria can adhere to particle sizes between 5-60 μm of diameter [28] while other researches establish that the risk stands with particle sizes of 10 μm which is equivalent to a squame dimensions [29]. These differences may be

due to different clothing materials or woven techniques used during the measurements [30]. Furthermore, bacterial loads on the skin may vary depending on the surgeons' and nurses' sex, age, nutrition status, personal health, and parts of the body that are exposed [31]. Several studies confirm that female personnel shed less amount of bacteria particles than males [32] and that old personnel disseminate more bacteria than young ones [33].

During the surgery, bacterial particles are suspended in the air and carried through the room by airflows [34]. Thermal plumes contribute to creating further fluctuations in the room's air distributions that can be beneficial or disadvantageous depending on the ventilation conditions [9]. For mixing ventilation systems, a strong thermal plume can prevent bacteria from going inside the wound and reduce infection [35]. However, for LAF systems, having a high plume that will later on be washed down, can lead to BCP depositing on the instrumentation table and causing a risk of infection when introducing these into the wound [36]. Thus, in LAF operating rooms with a
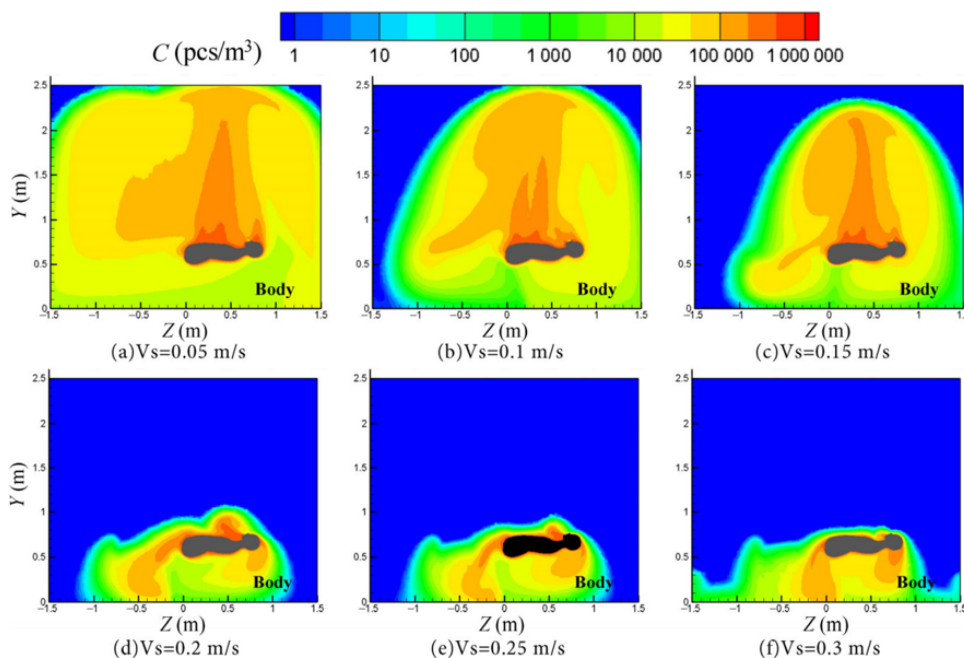
Figure 2.4: Particle concentration distribution in a LAF OR under different supply velocities. Source from [37]

supply velocity inferior to 0.25 m/s, thermal plumes can aggravate the infection risk [37]. Figure 2.4 illustrates the particle concentration transported by the thermal plume under different supply velocities in a unidirectional ventilation system. At the lowest initial velocity, the BCP concentration is spread to the entire critical zone maintaining the highest concentration above the stomach of the patient. As the velocity increases, the concentration diminishes, decreasing significantly the bacteria amount above the lying patient.

The cleaning effectiveness of the LAF system depends on the position of the surgical lamps and although it complies with the necessary supply velocity, the risk of SSI increases when situating an obstacle in between the unidirectional flow and the patient [23]. Figure 2.5 shows the velocity vector and BCP concentration distribution for a vertical unidirectional surgical room with surgical lamps close to the microenvironment zone.
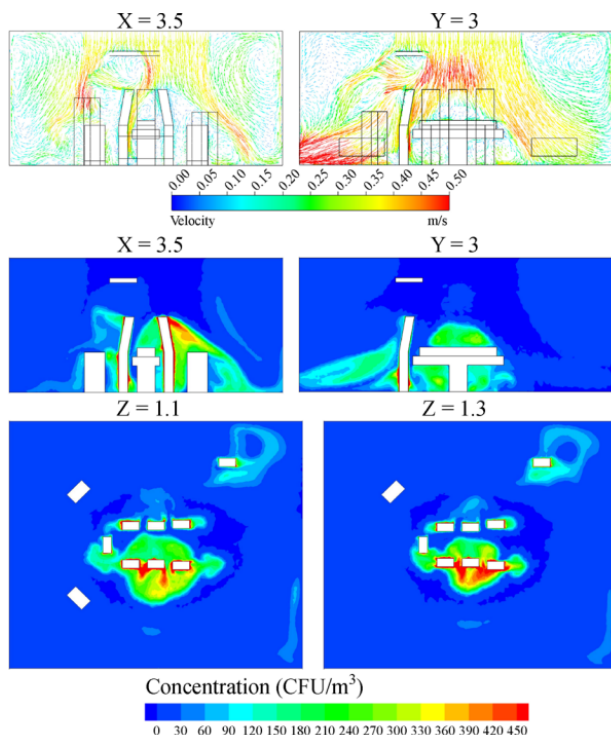
Figure 2.5: Particle concentration distribution in a LAF OR. Source from [38]

The supply air with an initial velocity of 0.25 m/s, is obstructed by the surgical lamp forming eddies, a swirl in the air stream, under it at 10 cm above the patient. High bacteria concentrations were also located above one of the instrument tables and behind the surgeons [38]. The surgeons' thermal plume and movement also take part in spreading the BCP and hence, an initial velocity of 0.25 m/s is not always enough to avoid bacteria around the critical zone.

The thermal plume is also affected by the clothing levels and by the breathing motion of the chest [39]. Furthermore, the surface area, temperature, and geometrical shape of the heat source are what cause the characteristics of the thermal plume [40]. As seen in Figure 2.6 the thermal plume can be divided into 3 regions, the initial, the self-similarity of mean motion, and the complete flow region. It can be seen that the plume becomes narrow at zone 1, meaning that the air accelerates away from the heat source [41]. The second region has an axisymmetric turbulent plume. For a setting without thermal stratification, a third region appears. Here the flow is complete and non-turbulent reaching the maximum plume [42].
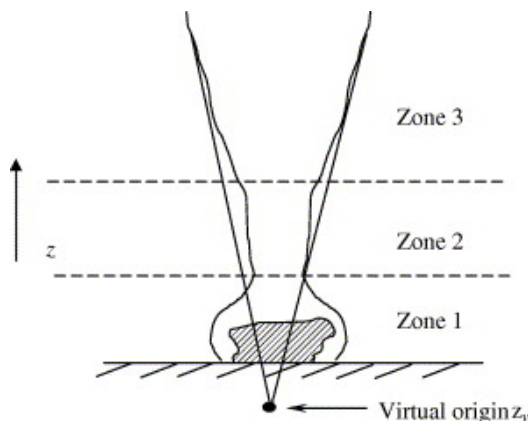
Figure 2.6: Different regions of a thermal plume. Source from [42]

2.4 Indoor environment specifications

The reasoning behind ventilation systems helping to reduce SSI has been addressed and thus, determining the minimum airflow is necessary. In addition, another prevention method is the enhancement of patients' immunity. Hypothermia commonly occurs in about half of all surgical patients and the effects of it can cause serious clinical consequences. A study showed that the risk of SSI was 9% higher in non-warmed patients [2]. Hence, the temperature and humidity in ORs should also be within determined limits to minimise infection risk while maintaining a comfortable thermal condition.

Hospital ORs are classified into different types of cleanrooms depending on their purpose. Technical standards and regulatory laws provide information on its construction, testing, cleanness, usage, and indoor specifications for the well-being of the patient as well as surgeons and nurses [14]. These requirements vary from country and thus, it is hard to determine which standard is more accurate and where to make improvements.
To be able to compare the air quality under dynamic conditions in different operating rooms from different hospitals, the University of Nashville has developed a set of environmental quality indicators that can evaluate the IAQ in ORs [43]. These indicators include air velocity, temperature, humidity, pressurisation, microbial data, and particle counting. The study discusses the advantages of using their method to make alterations in air changes per hour (ACH), filters, the usage of microbial sterilisers, and even the staff workflow to improve clinical outcomes while potentially reducing operating costs in hospitals.

To determine the required specifications for Norwegian hospitals, requisites for ORs in the US and European countries were studied as illustrated in Table 2.1, and the Norwegian specifications were determined by taking the overlapping intervals.These values will be later on compared with the conditions of the surgical rooms to determine if the current state of the ORs is safe for the patients and staff working there.

Table 2.1: Indoor environment standards for different countries in operating rooms

Country	Temperature [°C]	Velocity [m/s]	Humidity [%]	Airflow [ACH]	Pressure difference [Pa]	Standard
Spain	22-26	0.2-0.4	45-55	>20	5-20	UNE 100713 [44]
USA	20-23.8	Face air vel: 0.13-0.15 LAF	20-60	>20	>4	ASHRAE 170-2017 [45]
Germany	18-24	n.a.	50-60	>20	n.a.	DIN 1946 [46]
UK	18-28	0.3-0.38	35-60	>25	10-15	TM 03-01 [47]
France	18-26	LAF	n.a.	>50	10-20	AFNOR NF S90-351 [48]
Sweden	18-26	To be calculated >10 CFU/m^3	<70	To be calculated >10 CFU/m^3	>5	SIS-TS 39:2012 [49]
Romania	20-26	0.275	30-60	n.a.	n.a.	MLPAT indicativ C253-1-94 [50]
Italy	18-24	0.24-0.45	25-60	n.a.	>5	UNI CEN/TS 16244:2018 [51]
Norway	22-24	>3	50-55	>20	>10	n.a.

Chapter 3

Theoretical calculations

For the sole purpose of understanding the physics behind particle movement and how the room air can affect the patient's thermal plume to reduce SSI, equations are introduced in this section. A correction in the speed measuring devices was necessary and thus, the utilised equations are explained as well.

3.1 Speed correction for anemometers

The omnidirectional speed sensors provide measuring data for mean air speed, turbulence intensity, temperature, and standard deviation vectors.

For the calculation of the air velocity, readying only the mean air speed would be incorrect since a velocity vector is defined by the magnitude of speed and direction. The velocity will always be smaller than the mean air speed since the magnitude is always positive but the velocity vector can have both positive and negative values depending on its direction. For turbulent flow environments, this difference becomes greater, leading to considerable numerical mistakes when assessing the thermal plume [52]. Omnidirectional anemometers have been previously used for thermal plume studies and when calibrated and using the turbulence correction equations, the results were found to be accurate [42], [53], [54].

The magnitude of the mean velocity vector is defined by the values of the

15

velocity components of, V_x, V_y, and V_z as seen in Equation 3.1 [55].

$$\overline{V} = \sqrt{V_x{}^2 + V_y{}^2 + V_x{}^2} \tag{3.1}$$

One of the outputs of the omnidirectional sensor is the magnitude of the instantaneous velocity vector and averaging the given values provides the mean air speed [u_o], where t is the given time period as shown in Equation 3.2.

$$u_o = \frac{1}{t} \int_o^t \overline{V} \, dx \tag{3.2}$$

Furthermore, turbulence intensity is defined as the standard deviation of the velocity fluctuations divided by the magnitude of the mean velocity as seen in Equation 3.3 [40].

$$TI = \frac{SD}{\overline{V}} = \frac{\sqrt{\frac{1}{3}(V_x{}^2 + V_y{}^2 + V_z{}^2)}}{\overline{V}} \tag{3.3}$$

A valid equation for all turbulent air flows that can correct the speed of the measured anemometers into velocity vector is shown in Equation 3.4 [56].

$$TI = \sqrt{(1 + 3TI^2)\frac{\overline{V}^2}{u_o^2} - 1} \tag{3.4}$$

This equation was tested for different turbulence intensities and the ratio $\frac{u_o}{|V|}$ follows a simple parabolic equation at low TI, but at high turbulences, the ratio seems to be linear. Thus, the equation is divided into two as seen in Equation 3.5 and Equation 3.6 to properly obtain a correction formula at any given turbulence.

$$\frac{u_o}{V} = 1 + TI^2, \qquad TI \leq 0.45 \tag{3.5}$$

$$\frac{u_o}{V} = \frac{1.596TI^2 + 0.266TI + 0.3808}{0.173 + TI}, \qquad TI > 0.45 \tag{3.6}$$

16

3.2   Room average velocity calculations

For the calculation of the average velocity in a room, the kinetic energy model is used since it takes into account the influence of thermal plumes [57].

The conservation of kinetic energy can be expressed as Equation 3.7 where E_r is the room kinetic energy [J] and e the kinetic energy flux [J/s].

$$\frac{dE_r}{dt} = e_{input} - e_{output} + e_{sources} - e_{sinks} \tag{3.7}$$

Some potential energy flux parameters found in a room are listed below and can be calculated using Equation 3.8.

- **Energy inputs:** supply jets, infiltration, and gravity.

- **Energy outputs:** exhaust and exfiltration.

- **Energy sources:** heat sources, moving objects, boundary currents, or internal jets.

- **Energy sinks:** surface friction and viscous dissipation.

The supply jet energy flux is defined as Equation 3.8.

$$e_i = \frac{1}{2}\rho u_o^2 q \tag{3.8}$$

Where ρ is air density [kg/m^3], u_o initial velocity [m/s], and q volume flow rate [m^3/s].
The energy flux due to the heat source formula is displayed in Equation 3.9.

$$e_h = 5.3 \times 10^{-5}\rho\Phi_h(\Delta h + h_o) \tag{3.9}$$

Where Φ_h [W] is the convective heat flux from the source, Δh [m] is the distance from the heat source to the ceiling, and h_o [m] is the distance from the virtual origin of the thermal plume to the top of the heat source and it is calculated from Equation 3.10 where C is a constant = 4.18 and d [m] is the heat source diameter.

$$h_o = C \cdot \frac{d}{2} \tag{3.10}$$

Furthermore, the temperature difference between the supply and the room air produces a kinetic energy potential due to buoyancy [58]. This should be taken into account when estimating the room's average velocity and it can be calculated from Equation 3.11.

$$e_g = gHq_s(\rho_r - \rho_s) \tag{3.11}$$

Where g is the Earth's gravitational acceleration $[m/s^2]$, H is the height of the room [m], and ρ_r and ρ_s are the air densities at room and supply temperatures in kg/m^3.

Taking into account the kinetic energy balance equation, one can define the room average velocity equation as seen in Equation 3.2.

$$u_r = \frac{C_x^{\frac{1}{2}}}{\rho}\left(\frac{e_{input} - e_{output} + e_{source}}{0.664A_s}\right)^{\frac{1}{2}}\left(\frac{V_r}{A_s}\right)^{\frac{1}{6}} \tag{3.12}$$

Where u_r is the room mean velocity [m/s], $C_x = 1.4 \ m^{\frac{11}{3}}/s^{\frac{5}{3}}$ is an empirical coefficient, V_r is the room volume $[m^3]$ and A_s the area of the room surfaces $[m^2]$.

The energy fluxes from Equation 3.7 such as the infiltration and exfiltration through the envelope, and sink are not considered when calculating the room velocity, and the reason behind this is that the influence of these is very small compared to other energy fluxes and thus, it can be ignored [58].

Equation 3.2 has been validated by the company Halton Solutions [57] and Helsinki University of Technology [58] for mixing rooms and thus, it will be used in this study to calculate the average room velocity to evaluate the results.

Knowing the theoretical average velocity in a room can be useful to determine whether the enclosure is fully mixed or not. It is important in ORs that there are no stagnation zones and ergo the room is fully mixed to prevent

particles from concentrating in certain areas that could lead to infection risk.

3.3 Thermal plume calculations

Several methods of thermal plume calculations have been studied in previous years, however, most of them cannot predict asymmetrical plumes. Until now, the two most common methods known are the point heat source and the integral method [59]. Symmetrical plumes can be described with a Gaussian distribution curve using the following four parameters [40]:

- R_v - Width of the air velocity profile

- R_t - Width of air temperature excess profile

- v_{zm} - Maximum vertical air velocity component

- Δt_m - Maximum air temperature excess

The aforementioned parameters are not taking into account the inconsistency of the plumes profiles width, and hence, further integral characteristics (volume flux (V), momentum flux (I), buoyancy force density (P), and enthalpy flux (Q), also known as The Approximate Distributions Integration Method (ADI-method)), should be introduced [60], [61].

$$V = \sum v_i \cdot \Delta S \tag{3.13}$$

$$I = \rho \sum v_i^2 \cdot \Delta S \tag{3.14}$$

$$P = \rho g \beta \sum T_i \cdot \Delta S \tag{3.15}$$

$$Q = \rho \cdot c_p \sum (\Delta T_i \cdot v_i) \cdot \Delta S \tag{3.16}$$

Where ρ is the air density $[kg/m^3]$, g is the acceleration due to gravity $[m/s^2]$, β is the thermal expansion coefficient $[1/K]$, T_i is the excess air temperature [°C], v_i is the air velocity $[m/s]$, ΔS is the elementary area of the plume cross section $[m^2]$ and c_p is the specific heat of air $[J/kgK]$.

Furthermore, temperature excess distribution $(\Delta T(z))$ and air velocity $(v(z))$ at any given height (z) in asymmetrical thermal plumes can be expressed as follow [40]:

$$\Delta T(z) = \Delta T_m \cdot \exp -(\frac{r}{R_{t\alpha}})^n \tag{3.17}$$

$$v(z) = v_m \cdot \exp -(\frac{r}{R_{v\alpha}})^n \tag{3.18}$$

Where r is the radius distance from the plume axis [m] and $R_{t\alpha}$ and $R_{v\alpha}$ are the local angular widths of the air temperature excess and velocity profile respectively [m]. ΔT_m is the maximum air temperature excess [°C] and v_m is the maximum vertical air velocity component [m/s]. For symmetrical plumes, the exponent n=2 should be used, and for non-symmetrical TP, the power of n for both equations should be in the range between 1.5 and 2.

For the calculation of the radius as seen in Equation 3.19, it is necessary to first determine the plume axis wandering. This phenomenon occurs due to the convective boundary layer caused by the heat source or by alterations in the plume surroundings [62].

$$r = [(x - x_0)^2 + (y - y_0)^2]^{\frac{1}{2}} \tag{3.19}$$

The local angular width parameters are obtained by calculating the second harmonic function as seen in Equation 3.20 and Equation 3.21 where R_{t0} and R_{v0} are the mean widths for the temperature and velocity plume cross-section respectively. A visual understanding of the parameters is shown in Figure 3.1.

$$R_{t\alpha} = R_{t0}[1 + A_{t1}\sin(\alpha + \varphi_{t1}) + A_{t2}\sin(2\alpha + \varphi_{t2})] \tag{3.20}$$

$$R_{v\alpha} = R_{v0}[1 + A_{v1}\sin(\alpha + \varphi_{v1}) + A_{v2}\sin(2\alpha + \varphi_{v2})] \tag{3.21}$$

φ_1 and φ_2 are the phase shift angles while A_1 and A_2 are the amplitudes.
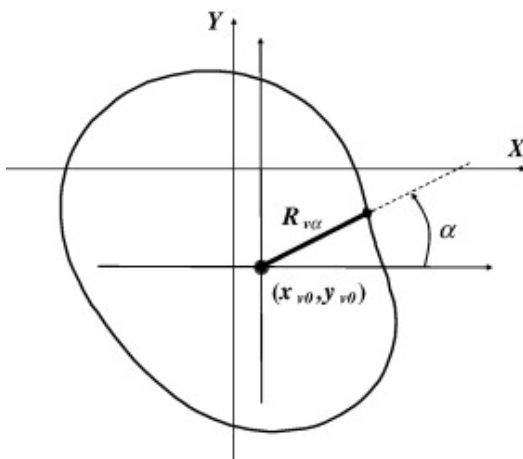
Figure 3.1: Illustration of the calculation of local angular parameters [40].

3.4 Particle motion

Airborne particles found in ORs, particularly the smaller ones, are affected by the local airflow and airflow streamlines [63]. Airflow behaviour is complex but crucial to understanding and predicting the movement of particles within a room, as small particles behave in the same manner as the airflow [64]. Studies noted that particles with diameter sizes between 0.1 and 1 μm did not show significant contrasting motion patterns unless the particles were approaching a surface [65]. For bigger diameters, the gravitational force dominates the particle motion, not following the airflow. Predominantly, particle dispersion is determined by the Stokes number (STK), and conceding that particles have STK $\leq$ 0.1 they will follow the airflow streamlines [66].

3.4.1 Turbulent airflow

As aforementioned, the airflow pattern is crucial to understand particle motion. A widely used method is the Realisable k-ε model that compasses the Reynolds-Averaged Navier-Stokes methods in addition to a turbulence kinetic energy (k) and dissipation rate (ε) as seen in Equation 3.22 [67]–[70].

$$\frac{\partial}{\partial t}(\rho\varphi) + \nabla \cdot (\rho\varphi\vec{V} - \Gamma_\varphi\nabla\varphi) = S_\varphi \tag{3.22}$$

where ρ is the air density, φ denotes the transported quantity, $\vec{V}$ is the velocity vector, S_φ is the source term and Γ_φ the effective diffusion coefficient for each dependent variable.

This model is only valid to estimate the part of the room that is strongly turbulent since this method assumes isotropic turbulence. Therefore, it would be inaccurate to simulate the airflow close to surfaces with this eddy viscosity model [41].

3.4.2 Lagrangian particle tracking method

As bigger particles do not follow the airflow pattern, different equations must be considered for these contaminants. There are two particle tracking methods to simulate particle diffusion in a room: Eulerian particle tracking (EPT) and Lagrangian particle tracking (LPT), although studies have demonstrated that the LPT method appeared to be more accurate [36].

This Lagrangian tracking method calculates particles' individual trajectories through the momentum equation as expressed in Equation 3.23 [71].

$$\frac{dV_p}{dt} = F_D(V - V_p) + \frac{g(\rho_p - \rho)}{\rho_p} + F_B + F_{therm} + F_s \qquad (3.23)$$

where $\frac{dV_p}{dt}$ represents the inertial force and $F_D(V - V_p)$ the drag force per unit particle mass. V is the velocity vector and g is the gravitational acceleration. $\frac{g(\rho_p - \rho)}{\rho_p}$ is the gravitational and buoyancy force while F_B is the Brownian force, F_{therm} refers to the thermophoretic term and F_s is the Saffman's lift term.

The drag force can be further expressed as Equation 3.24 and it is the most significant force [72].

$$F_D = \frac{18\mu}{\rho_p d_p^2} \frac{C_d Re_p}{24} \qquad (3.24)$$

where μ is the molecular viscosity of air, d_p is the particle diameter, Re_p is the Reynolds number based on the diameter of the particle, C_d is the drag coefficient for spherical particles which can be obtained from Equation 3.25

[73].

$$C_d = \frac{\xi_1}{Re} + \frac{\xi_2}{Re^2} + \xi_3 \qquad (3.25)$$

where ξ are constants.

One of the limitations of the LPT method is that it does not calculate particle concentration hence, the discrete random walk (DRW) model is adequate to simulate the fluctuating velocity (u') following a Gaussian probability distribution as seen in Equation 3.26 [72].

$$u' = \psi\sqrt{u'^2} = \psi\sqrt{\frac{2k}{3}} \qquad (3.26)$$

where ψ is the normally distributed random number. Due to the random number, uncertainties regarding the particle concentration may occur and to obtain statically reliable results, several trajectories need to be simulated [74].

3.4.3 Particle deposition

The deposition of contaminants around the microenvironment area could potentially lead to SSI and thence it is important to take it into account [75] The particle deposition velocity, v_d, is modelled by assuming that the airflow of the room is homogeneous and isotropically turbulent. It takes into account the Brownian force, turbulence diffusion, and gravity. In addition, it comprises both horizontal (Equation 3.27 and Equation 3.28) and vertical surfaces (Equation 3.29) [76].

$$\frac{v_d}{u^*} = \frac{\frac{v_s}{u^*}}{1 - exp(-\frac{v_s}{u^*}I)}, \qquad Upwards \qquad (3.27)$$

$$\frac{v_d}{u^*} = \frac{\frac{v_s}{u^*}}{exp(-\frac{v_s}{u^*}I) - 1}, \qquad Downward \qquad (3.28)$$

$$\frac{v_d}{u^*} = \frac{u^*}{I}, \qquad Vertical \qquad (3.29)$$

where u^* is the friction velocity, v_s the particle settling velocity and I is expressed as Equation 3.30 [77].

$$I = \int_{r^+}^{30} \frac{v_g}{\varepsilon_p + D_p} \, dy^+ \tag{3.30}$$

where $y^+ = \frac{xu^*}{v_g}$ and $r^+ = \frac{d_p}{2} \frac{u^*}{v_g}$. Furthermore, ε_p stands for the particle eddy diffusivity, D_p is the Brownian diffusivity of the particle, v_g is the kinetic air viscosity and x is the distance between the wall and the first cell center. Other recent studies have improved this model by adding the effect of turbophoresis [78].

Chapter 4

Methodology

Four 40 minutes mock-up surgeries in two operating rooms at St. Olavs Hospital were performed to study the influence of the room temperature on a patient's thermal plume. The cases encompassed two different temperatures, 21 °C and 23 °C, and two ventilation systems, mixing and laminar airflow.

4.1 Mixing ventilation operating room

The OR with mixing ventilation had an area of 59.1 m^2 and a height of 2.9 m. The surgical bed is placed approximately at the centre of the room as seen in Figure 4.1.

Figure 4.2 demonstrates the overview of the mixing ventilation system, which is composed of an inlet duct (blue and red) and two exhaust outlets (green). The air that is introduced into the operating room from the AHU (Air handling unit) passes through a temperature-controlled heating coil regulated by a valve to achieve the desired values. A water-based surface air cooler is also utilised when the supply air is desired to be lower. The air passes through a damper to control the amount of airflow needed in the room before being filtered from pathogens and particles. The red duct is in reality divided into 4 inlet points and during the measurements, they were each located at 3.9 m, 4.2 m, 3 m, and 3.4 m from the wound.

Figure 4.1: Image of the mixing ventilation operating room at St. Olavs Hospital where the measurements took place.

The exhaust air was divided into going back to the AHU or the outdoors. The duct towards the AHU measured the temperature and relative humidity of the air before passing it through a damper while the other exhaust outlet solely had a volume control damper.
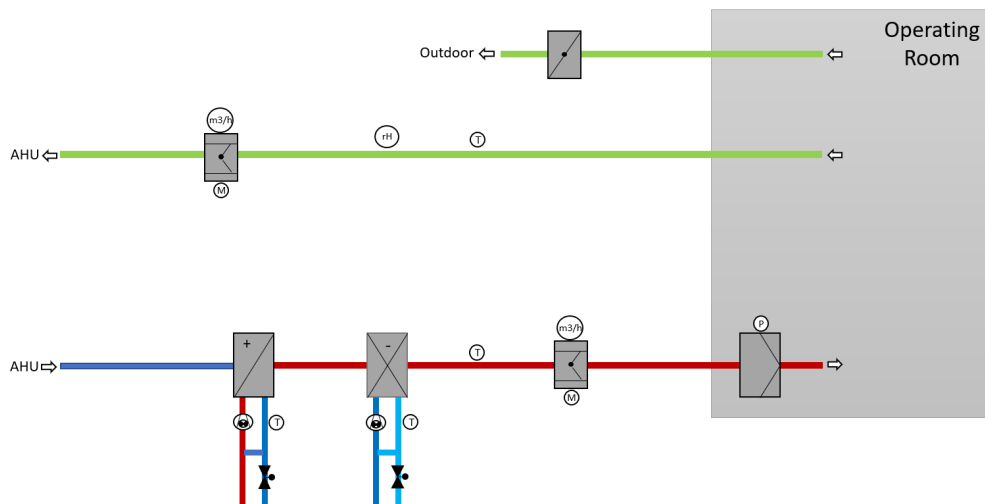
Figure 4.2: Mixing ventilation system with intensive treat fresh air system used in the operating room. Sketch provided by St. Olavs Hospital.

4.2   Laminar airflow operating room

The laminar operating room had a total area of 56.1 m^2, of which 11 m^2 is the rectangular LAF zone, with a room height of 3.08 m. The surgical bed was positioned at the centre of the LAF zone as seen in Figure 4.3.

Figure 4.3: Image of the Laminar airflow operating room at St. Olavs Hospital where the measurements took place.

The ventilation system of the LAF is composed of a returning air duct with heat recovery and as seen in Figure 4.4, before introducing the air into the OR (blue and red duct), the air from the AHU passes through a damper that controls the amount of airflow and which is controlled by a motor. It is then followed by a filter with a pressure difference sensor to collect unwanted pathogens and particles. The fan with a pressure sensor is in charge of moving the air through the duct toward the heating coil and the surface air cooler. These are used to reach the desired temperatures in the OR. Finally, before entering the surgical room, the air passes through another filter to make the air as clean as possible.

The remaining green ducts are the exhaust outlets. One of them is the recirculating duct that is connected to the inlet duct and recirculates around 71 % of the operating room's air. A second exhaust duct returns to the AHU passing through a damper and ultimately, the last green duct excesses some air into the corridor through the volume control damper.

Temperature, airflow, pressure difference, and relative humidity sensors are placed along the system for better control of the flow and indoor parameters of the OR.
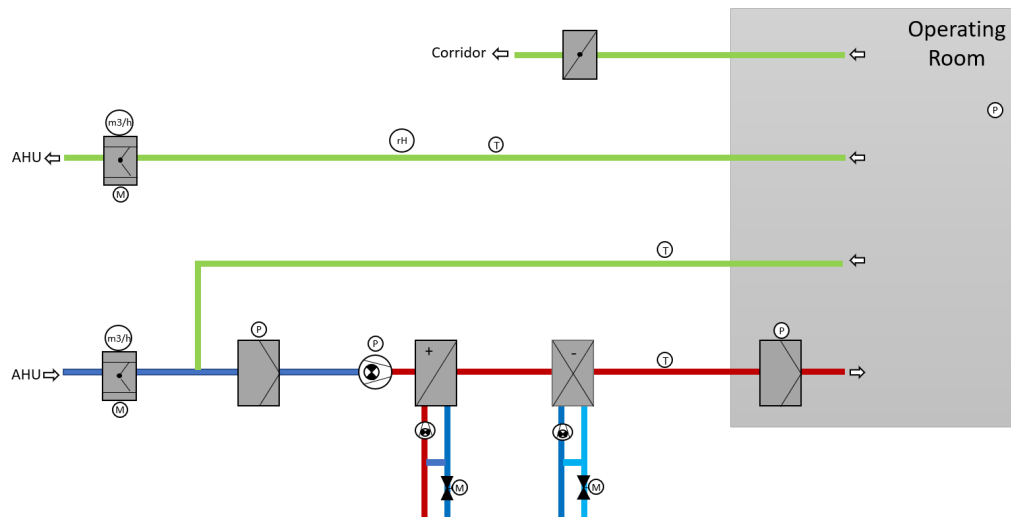
Figure 4.4: LAF ventilation system with heat recovery used in the operating room. Sketch provided by St. Olavs Hospital.

During the measurements, the measured supply velocity into the operating room was 0.3 m/s which is within the desired values [10] and the wound was at a distance of 2 m from the ceiling and 1.08 m above the floor.

4.3 Instrumentation

An overview of the instrumentation used for the mock-up surgeries is illustrated below since the proper understanding of the use and limitations of the measuring instruments are crucial to properly analyse the data.

4.3.1 Anemometers to measure velocity and turbulence intensity

SensoAnemo 5100 LSF omnidirectional anemometers were used in order to measure the speed and turbulence intensity at different heights above the

wound and record data every 2 seconds. These devices can measure the speed between 0.05 and 5 m/s with an accuracy of speed of ±0.02m/s and $\pm1\%$ of readings. [79]. These anemometers were calibrated in December 2020 as can be seen in chapter A

Figure 4.5: Image of SensoAnemo 5100 LSF from sensor electronics. Picture obtained from [79]

4.3.2 Temperature and relative humidity

Tinytag Plus 2 was used to measure the room temperature and relative humidity. It has a temperature reading scale of -25 to +85 °C and a reading resolution of 0.01 °C and its accuracy depends on the measured temperature as seen in Figure A.1. Regarding the relative humidity, it has a measuring scale from 0 to 100% and an accuracy of $\pm3.0\%$ RH at 25 °C [80]. The time interval during the surgery was of 10 seconds and they were placed on the operating table, supply inlet, and exhaust outlet.

Figure 4.6: Image of Tinytag Plus 2 — TGP 4500 from Gemeni data loggers. Picture obtained from [80]

4.3.3 Heat source

A 1.7 m tall female humanoid thermal mannequin was used as a patient for every scenario. The core temperature of the mannequin was kept within a range of 33.5 - 34.5 °C for all scenarios and was not wearing any surgical clothing, only covered by the surgical blanket, to simulate a realistic patient during surgery. The chosen temperature range was determined by previous studies which stated that within the experiment's conditions, the temperature range should be between 32 - 34 °C [81], [82]. The power output of the mannequin could vary between 0-200 W and the heat points were placed on the head, arms, core, and legs.

Figure 4.7: Image of the female humanoid thermal plume.

4.3.4 Infrared camera

The infrared camera, Flir One - iOS, was remarkably easy to use and transport due to its compact size and clear instructions from its app. It requires to be connected to an iPhone and through the mobile's camera, it captured the temperature ranges within the room. It has an accuracy of ± 3 °C for scenes within 15 °C to 35 °C. The emissivity was adapted to the mannequin's properties and the battery life of the device was 1 h, hence it had to be charged between measurements [83].

Figure 4.8: Image of infrared camera Flir One - iOS. Image obtained from [83].

4.3.5 Variable transformer

The voltage variable transformer was used to control the power output of the mannequin. It had a voltage range between 0 to 260 and by spinning the black wheel, it could be changed to a different setting. This is seen in Figure 4.9 where the voltage value was set to the desired constant one during the measurements.

Figure 4.9: Voltage variable transformer used during the measurements to correct the output power of the thermal mannequin.

4.3.6 Energy cost meter

The variable transformer controlled the output voltage, however, in order to confirm the power output, the GAO EMT707CTL energy cost meter was used. It has an accuracy of $\pm 5.0\%$ and has the possibility to measure voltage, amperes, hertz, watts, apparent output, and kilowatt hours [84].

31

Figure 4.10: Image of energy cost meter - GAO EMT707CTL. Image obtained from [84].

4.3.7 Thermal detector

Precautions were made to ensure that the mannequin conditions were optimal and so, a Bosch PTD 1 thermal detector capable to assess surface temperature was used to measure the core temperature of the patient. The pistol has a temperature accuracy of ± 3 °C for scenes between 10 °C and 30 °C. The emissivity degree was changed to *High emissivity degree* of 0.95 due to the properties of the surface of the mannequin. The measuring distance was 0.5 m for desirable results [85].

Figure 4.11: Image of thermal detector - Bosch PTD 1. Picture obtained from [85].

4.3.8 Laser meter

To measure the height of the anemometers to the wound, a digital meter was used. It has a minimum measurement of 1 mm and an accuracy of ± 3 mm with a measuring range between 0.15 - 20.000 m [86]. A conventional tape meter was used for the same objective as well.

Figure 4.12: Image of the Bosch Zamo laser measure. Picture obtained from [87].

4.4 Experimental set-up

Two operating rooms with different ventilation systems, laminar airflow, and mixing ventilation, were used as case studies to perform a thermal plume measurement under two different room temperatures, 21 °C and 23 °C. A thermal mannequin was placed in an operating bed to simulate a patient under stomach surgery. The mannequin was not wearing any clothing and was covered by a surgical blanket to obtain realistic results. In addition, the blanket was cut into the shape of a 20 cm square and to avoid fluctuation of the thermal plume, the sides of the surgical blanket were taped to the mannequin as seen in Figure 4.13a. Moreover, the taping provided a constant thermal plume throughout every measurement since the study area was unchanging for every scenario. To keep the measurements comparable, a reference point was placed at the centre of the core where the stomach of the patient would be located. A red arrow pointing to this point is shown in Figure 4.13b.
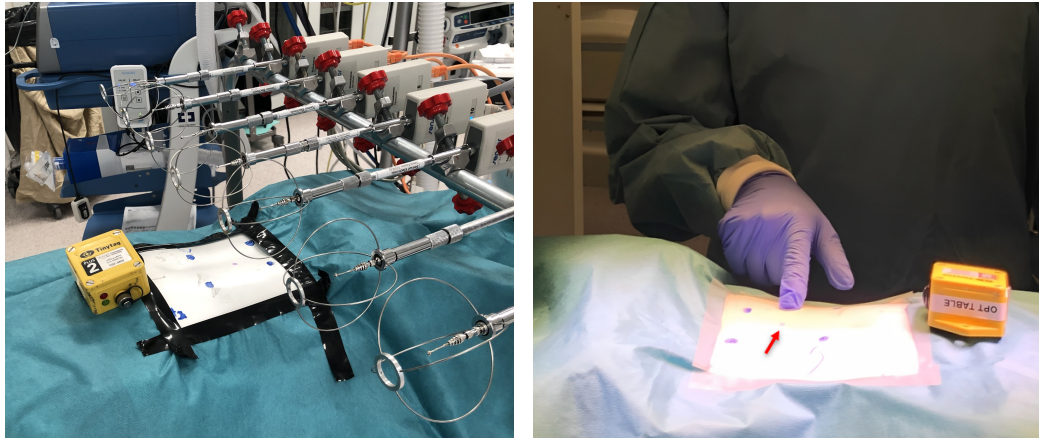
(a) Tape around the assumed wound.   (b) Reference point.

Figure 4.13: Set-up of the patient for the anemometers measurement.

A total of seven anemometers, 8.5 cm apart, were attached to a support rack that could be moved vertically to five positions with different heights, placing the 4th anemometer above the reference point. The aforementioned layout is portrayed in Figure 4.14. The chosen heights were 5, 10, 25, 50, and
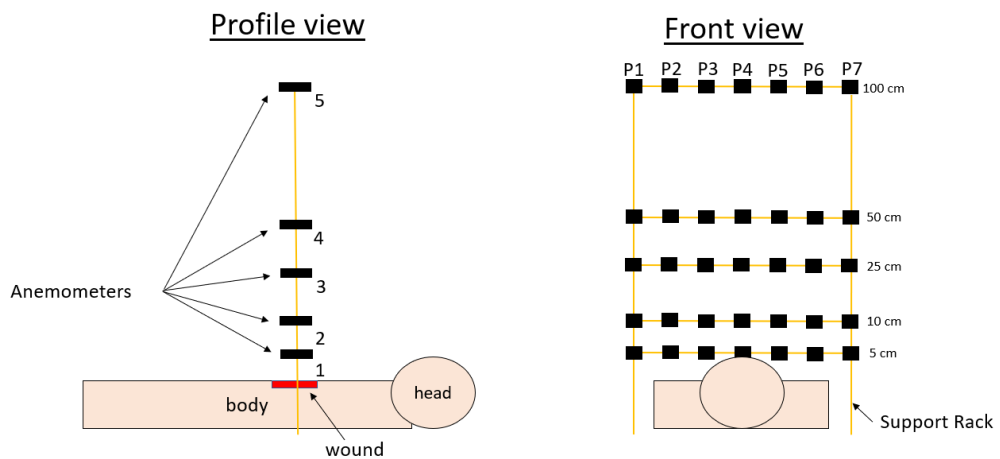
Figure 4.14: Measurement layout that took place in all 4 scenarios.

100 cm above the wound. The reasoning behind choosing only 5 heights was to be able to combine this project with an ongoing project at St. Olavs and due to timing restrictions, the measurements for this study had to maximum

last 1 hour. Within this time, the OR was set up, 5 different heights of 5 minutes each were measured, and the operating room was left ready for the next study.

Due to the different phenomena happening in the mixing vs laminar ventilation, the heights were decided to be between 5 cm above the wound, as it is the lowest possible measurement due to the physical shape of the anemometer and bust of the mannequin, and 100 cm above the wound since this was the maximum height the supporting rank could achieve. For LAF thermal plumes with supply airflow of 0.3 m/s, the maximum height is reached at 50 cm and the height where more eddies appear is between 10-25cm [37]. For these reasons, the chosen heights were crucial for the study. Figure 4.15 illustrates the maximum and minimum measured height in the two operating rooms.

(a) 100 cm above the wound in the MV OR.

(b) 5 cm above the wound in the LAF OR.

Figure 4.15: Measurement set-up for 100 and 5 cm above the wound.

4.4.1 Temperature control

During the first measurement, the thermal mannequin was giving faulty power outputs of around 114 W when it should have been 40 W. This meant a higher thermal output and hence an unrealistic increase in the thermal plume. The first measurements could not be used in this study due to the lack of credibility, however, it introduced a problem that needed fixing. The mannequin was taken to the universities workshop to run several tests and figure out what were the roots of the problem and how to fix it. After a few weeks, The problem was found to be the power controller located at the back of the mannequin and so it was changed and equipped with a new potentiometer.

Meanwhile, the tight measurement schedule required a faster alternative, and therefore a variable transformer was used to control the output voltage. Variable transformers are devices that can transmit different amounts of output voltage from the same input voltage [88]. The variable transformer was connected to the mannequin and the energy cost meter that could measure volts. The reason behind this was to ascertain the thermal conditions necessary to simulate a real patient under surgery. Once the equipment was connected, the voltage could be adjusted with the black rotating wheel. Fig-

Figure 4.16: Connections to the variable transformer.

ure 4.16 illustrate the discussed connections where the black cable is attached to the mannequin and the white one coming from the variable transformer, is the one connected to the voltmeter.

To corroborate the mannequin's thermal discharge, a thermal detector, and infrared camera were used. The measuring temperature point was the same as the anemometers reference point seen in Figure 4.13b. Due to the big temperature accuracy of both devices, ± 3 °C in comparison to the small measuring range, 33.5-34.5 °C, the utilisation of the two instruments was desired. Figure 4.17 compares the temperature difference measured by both apparatuses. for Figure 4.17b, the reference point is determined by point 2 which is only 0.4 °C lower than the one measured by the thermal pistol. The results of both devices were satisfactory and they were used throughout the study to estimate the core temperature of the mannequin. To control the temperature within the mentioned range, the wheel on the variable transformer was rotated until reaching acceptable temperatures.

(a) Temperature measured by thermal pistol
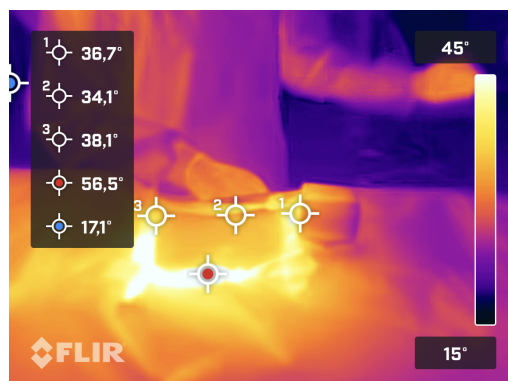
(b) Temperature measured by thermal camera

Figure 4.17: Comparison of mannequin body temperature measured with a thermal pistol and a thermal camera.

4.4.2 Experimental method

Both operating rooms have 20 air changes per hour (ACH) which means that it takes 3 minutes for new air to be introduced. Opening and closing the doors can affect not only the pressure within the room but also the air distribution. Another factor that can contribute to disturbing the air distribution in the room is performing any sort of movement. Hence, before taking the measurements, it was important that the door was closed and the people within the room were either standing or sitting still away from the microenvironment area. A waiting time of 6 minutes took place after the mentioned conditions were met.

Two people were required to move the support rack to different heights to avoid any risk of harming the anemometers and to obtain a more precise horizontal measurement. Although a level tool was used for this, having two people, accelerated the process and confirmed the correct rack position. The laser meter or a conventional tape meter was used to measure the distance between the 4th anemometer and the reference point as seen in Figure 4.18.
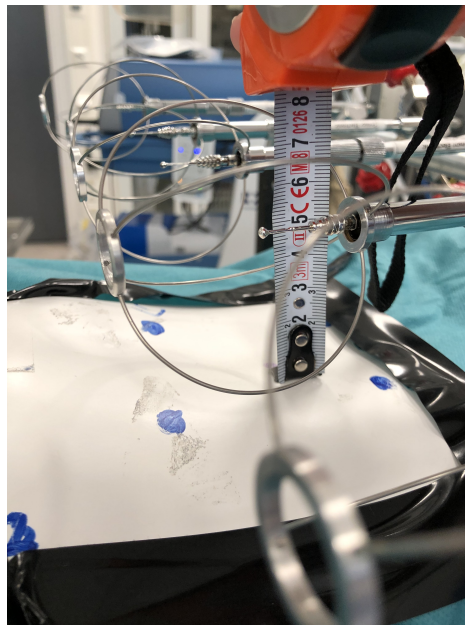
Figure 4.18: Measuring 5 cm above the wound with a tape meter.

To solely determine the thermal plume of the mannequin in the room

and how it is influenced by the ventilation system, the surgical lights were turned off. Another reason behind not using the lights was that they might have become an impediment in the study due to acting as an air distribution barrier over the studied area.

Previous studies have shown the importance of using a humanoid shape to determine the thermal plume rather than a cylinder or a rectangular box. Using a mannequin conveyed the TP to be asymmetrical and the axis of the TP changed [61], thus obtaining more authentic results. A constant power output was achieved by setting the variable transformer at 60 W which corresponded to the sought wound temperature.

The cases performed during this study are represented in Table 4.1.

Table 4.1: Measuring cases.

	Type of ventilation	Room temperature [°C]	Supply temperature [°C]	ACH
Case A	MV	21	18.9	20
Case B	MV	23	23.3	20
Case C	LAF	21	21.6	20
Case D	LAF	23	22.8	20

Chapter 5

Results

The measured and analysed parameters that encompass the result section include the indoor parameters in the ORs: pressure, temperatures, and humidity, to compare it with hospital indoor environment standards. Moreover, velocity, temperature, and TI profiles were presented to explain the performance of the thermal plume under different circumstances as well as a calculation subsection using the equations explained in chapter 3. The following results were analysed using the Matlab scripts found in chapter B.

5.1 Indoor environment parameters inside the operating room

The indoor air parameters were measured using Tinytags to evaluate the conditions of the operating rooms and compare them with the aforementioned standards Table 2.1.

For the MV OR, Figure 5.1, one can observe that the room temperature of 21 °C is more stable than 23 °C. At the beginning of the measurement, the 23 °C room temperature did not achieve its required value, however, if only the data after 10 minutes of mock-up surgery are taken into consideration, the fluctuation of the blue dotted line is 0.3 °C while the other temperature does not reach 0.1 °C. Regarding the humidity, it seems that both scenarios
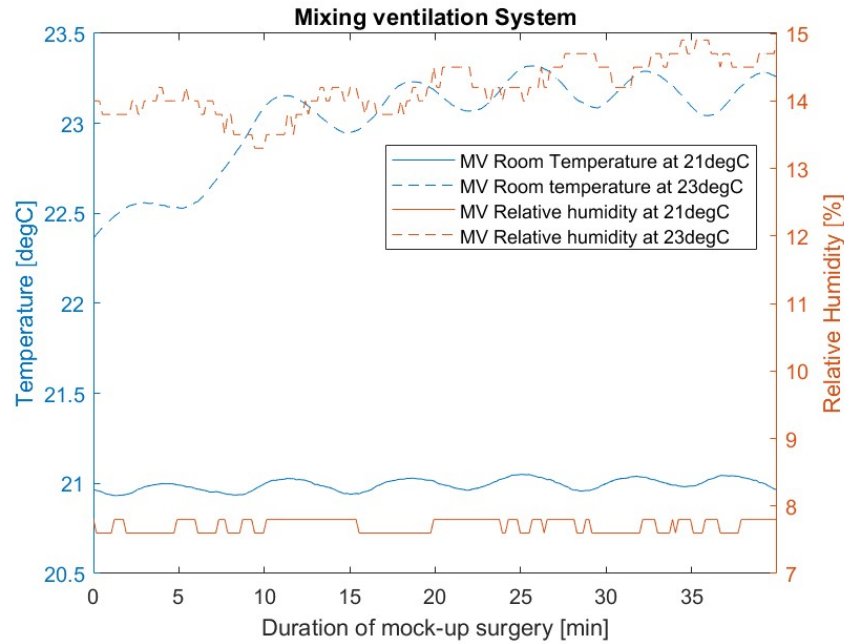
Figure 5.1: Indoor air parameters in the mixing ventilation room.

have lower values than what the standards suggest, having a maximum relative humidity of 7.8 % for the 21 °C room temperature and 14.9 % for the 23 °C.

Furthermore, for the LAF OR, Figure 5.2, the temperatures are quite stable for both cases, keeping a stable value of 21.6 and 22.8 °C respectively. An increase in relative humidity is also seen as the temperature increases, such as with the MV scenarios. The relative humidity for 21 °C is higher than with the mixing ventilation, reaching a value of 11.6 % while for the 23 °C the highest measured value was 13.5 %.

The airflow rate of the mixing room is displayed in Figure 5.3 where it can be seen that the OR was kept at positive pressure to protect the patient during surgery. Most ORs are either kept at positive pressure to avoid pathogens from entering the theatre or at negative pressure to avoid infection from spreading [89]. Having a greater amount of supply air than exhaust air
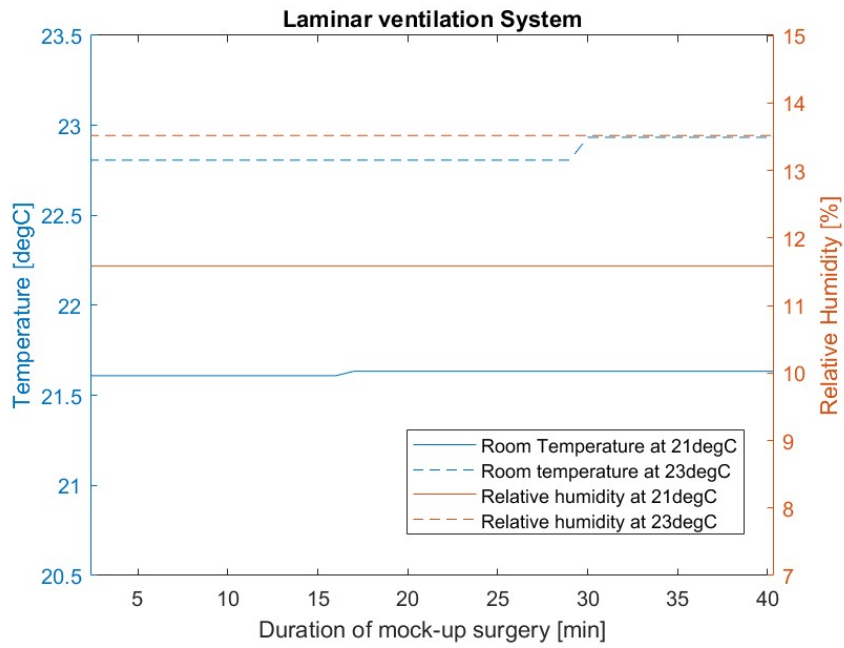
Figure 5.2: Indoor air parameters in the laminar ventilation room.
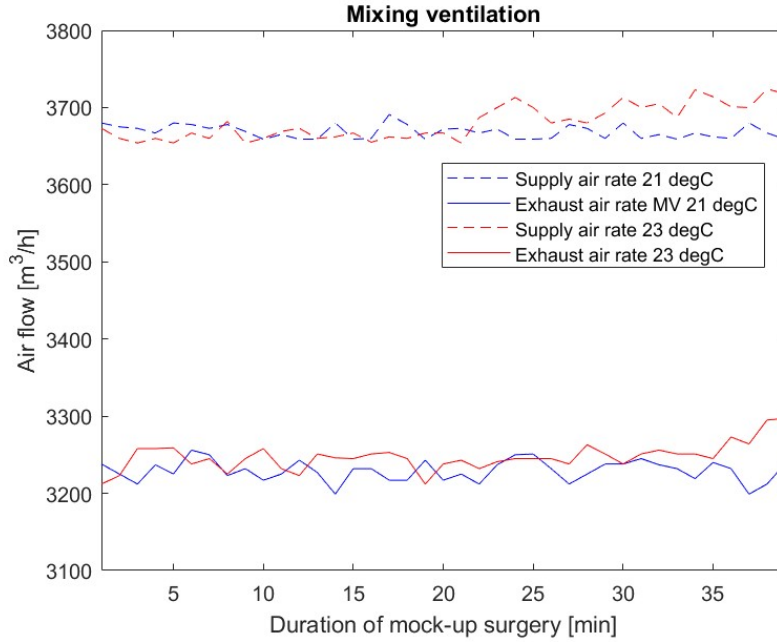
Figure 5.3: Airflow parameters in mixing operating room.

results in a positive pressure environment and this is the case for all four scenarios portrayed in this study. For the 23 °C case, the room required a slightly greater amount of airflow of 3681.9 m^3/h while the supply of 21 °C was 3668.5 m^3/h. In order to keep a similar pressure difference in the room at all times, the exhaust flow of the former case was also higher than the latter, 3249.5 and 3228.7 m^3/h, respectively.
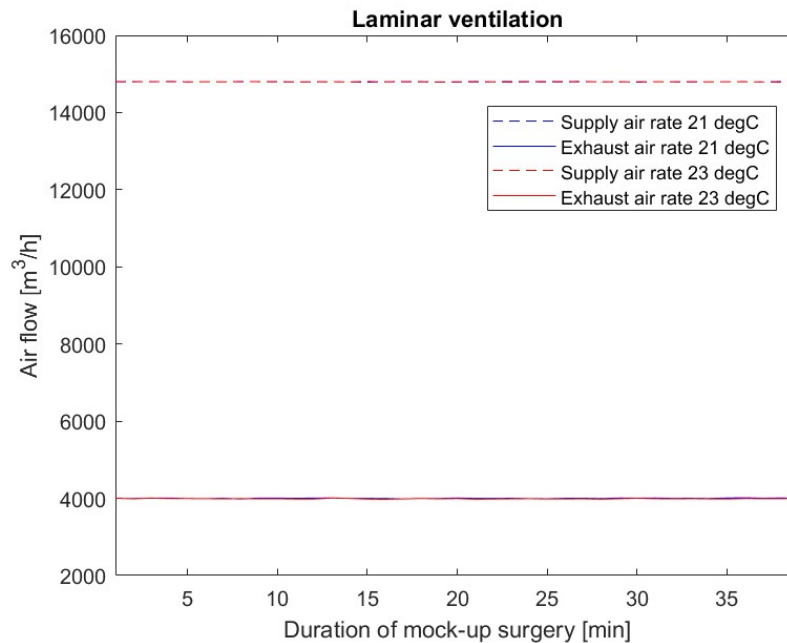
Figure 5.4: Airflow parameters in the laminar operating room.

The airflow rate of the LAF OR is shown in Figure 5.4 where it can be seen that the supply airflow is kept at 14806 m^3/h for both temperatures while the exhaust flow for cases C and D were 4013.6 and 4005.9 m^3/h respectively. The supply is composed of approximately 30 % new air from the AHU and the remaining is recirculated air. A more detailed overview of the supply airflow is shown in Figure 5.5 where 4300 m^3/h of new air is introduced and 10500 m^3/h is recirculated air.
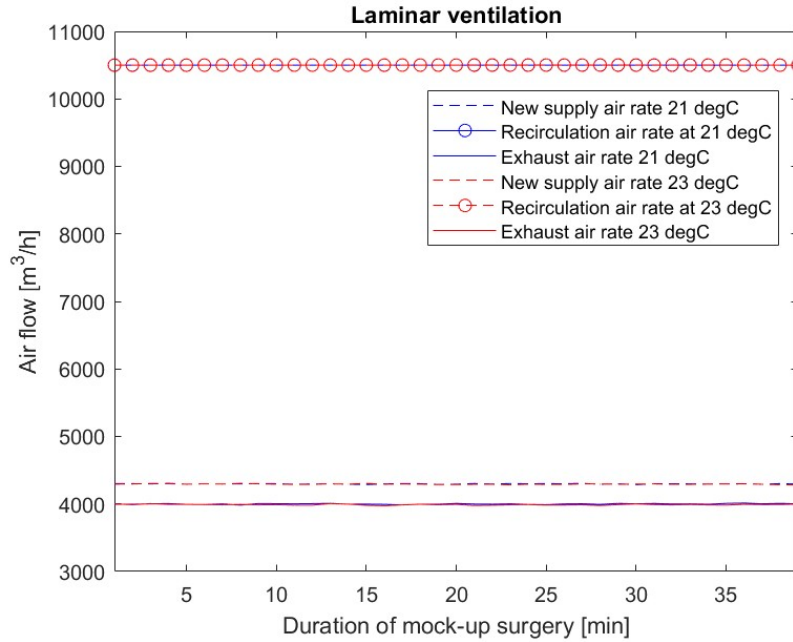
Figure 5.5: Detailed airflow parameters in the laminar operating room.

5.2 Velocity profiles

The raw data, measured with the omnidirectional anemometers, were corrected using the speed correction Equation 3.5 & Equation 3.6, and later on the results were analysed using the MATLAB *countourf* function that interpolates the data to be able to obtain a more visually-friendly chart as seen in Figure 5.6. As shown in Figure 4.14, the wound is positioned at the centre of the x-axis, the table's width, which corresponds to 0.3 m in the charts.

The first two cases, A & B, refer to MV and thus, the velocity values are smaller than with the cases C & D which correspond to LAF. The thermal plume for the first scenario, Figure 5.6a, has the highest velocity at 10 cm above the wound. The thermal plume's velocity decreases as it gets farther away from the wound and mixes with the room air. As seen in Table 5.1, the calculated theoretical average room velocity of 0.107 m/s is very similar to the one measured by the anemometers 0.11 m/s and from the chart, the thermal plume reaches this velocity at height 100 cm.

For the second case, Figure 5.6b the velocities are clearly lower than in

45

(a) Mixing ventilation at 21 °C

(b) Mixing ventilation at 23 °C

(c) Laminar ventilation at 21 °C

(d) Laminar ventilation at 23 °C
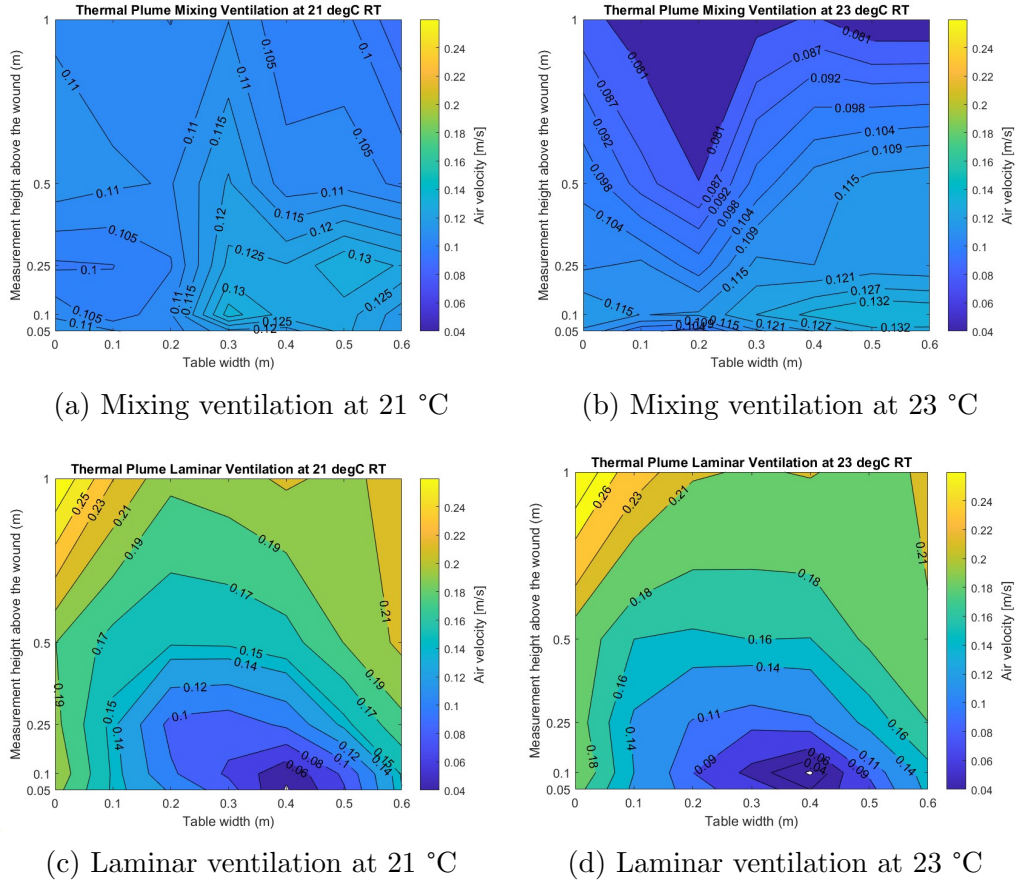
Figure 5.6: Velocity profile of the patient's thermal plume.

the previous scenario. The room temperature in this case is 2 °C higher and therefore the temperature difference between the thermal plume and room air is smaller. From Equation 5.1 it can be understood that assuming an ideal gas, the density of the air would decrease with a higher room temperature.

$$\rho = \frac{MP}{RT} \tag{5.1}$$

Where M is the molecule mass of the gas [g/mol], P is the pressure of the gas [atm], R is the gas law constant and T is the gas temperature [K]. This confirms that the air density between the thermal plume and room temperature is more similar and from the ADI-Method, Equation 3.15, we can understand that the buoyancy force is smaller than for the first case.

46

The similarities in air densities between the room's air and the TP signify better mixing [90], and since the buoyancy effect is not as predominant as in case A, the thermal plume is shorter and slower in comparison.

The other LAF scenarios show a different chart pattern. The velocities are highest farther away from the wound since it is closest to the unidirectional supply of air and as it gets closer to the wound, the velocities decrease. The velocities at 5 and 10 cm above the wound are the smallest seen in Figure 5.6c and Figure 5.6d due to the fact that the TP opposites the unidirectional flow and the resulting measured velocity is expressed as Equation 5.2.

$$v = v_{supply} - v_{TP} \qquad (5.2)$$

Where v_{supply} is the supply velocity and v_{TP} is the thermal plume's velocity.

5.3 Temperature profiles

The temperature profiles were analysed using the same method as the velocity profiles. These results show a visualisation of the physical characteristics of the thermal plumes and how they are affected by the change in room temperature.

Comparing Figure 5.7a to Figure 5.7b it can be seen that the TP for case A appears to reach a higher height while keeping a narrower width. Furthermore, for the LAF scenarios, a similar pattern is shown. The TP is wider and higher for case C, Figure 5.7c, than for case D, Figure 5.7d.

For cases C & D the TP is suppressed by the supply airflow, and due to the stronger buoyancy force for case C, the thermal plume has the strength to be able to reach a higher height. As a consequence, the TP for the last case is shorter but it widens close to the operating table. A comparable phenomenon happens for cases A & B except that the unidirectional flow does not act upon the thermal plume and thus, it can reach higher.

A tendency seen in every case is the second peak on the right of the TP. The interpretation behind this is that while taking the measurement, a hole

(a) Mixing ventilation at 21 °C

(b) Mixing ventilation at 23 °C

(c) Laminar ventilation at 21 °C

(d) Laminar ventilation at 23 °C
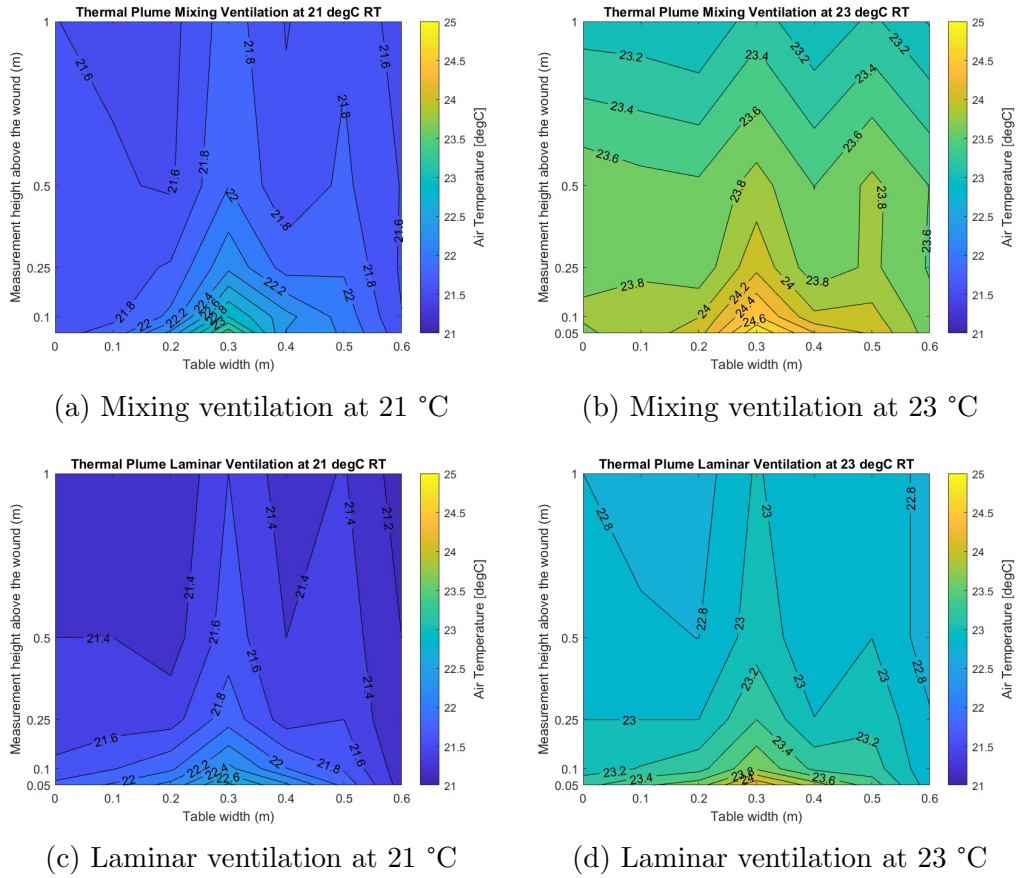
Figure 5.7: Temperature profile of the patient's thermal plume.

was cut into the surgical blanket to resemble a realistic operating wound. Due to the constant rearrangement of the mannequin into different ORs and to be able to compare the data between the four cases, tape was used to prevent the blanket from moving. Nevertheless, the heat of the patient resulted in the adhesive tape detaching from the right side which resulted in body heat escaping from under the blanket at high speed. This can be seen in Figure 5.6 where higher velocities are seen on the right side of the plume.

5.4 Turbulence Intensity profiles

The turbulence intensity charts display the velocity fluctuations. The different buoyancy forces and the suppressed TP for the LAF cases can also be seen in Figure 5.8.

(a) Mixing ventilation at 21 °C

(b) Mixing ventilation at 23 °C

(c) Laminar ventilation at 21 °C

(d) Laminar ventilation at 23 °C
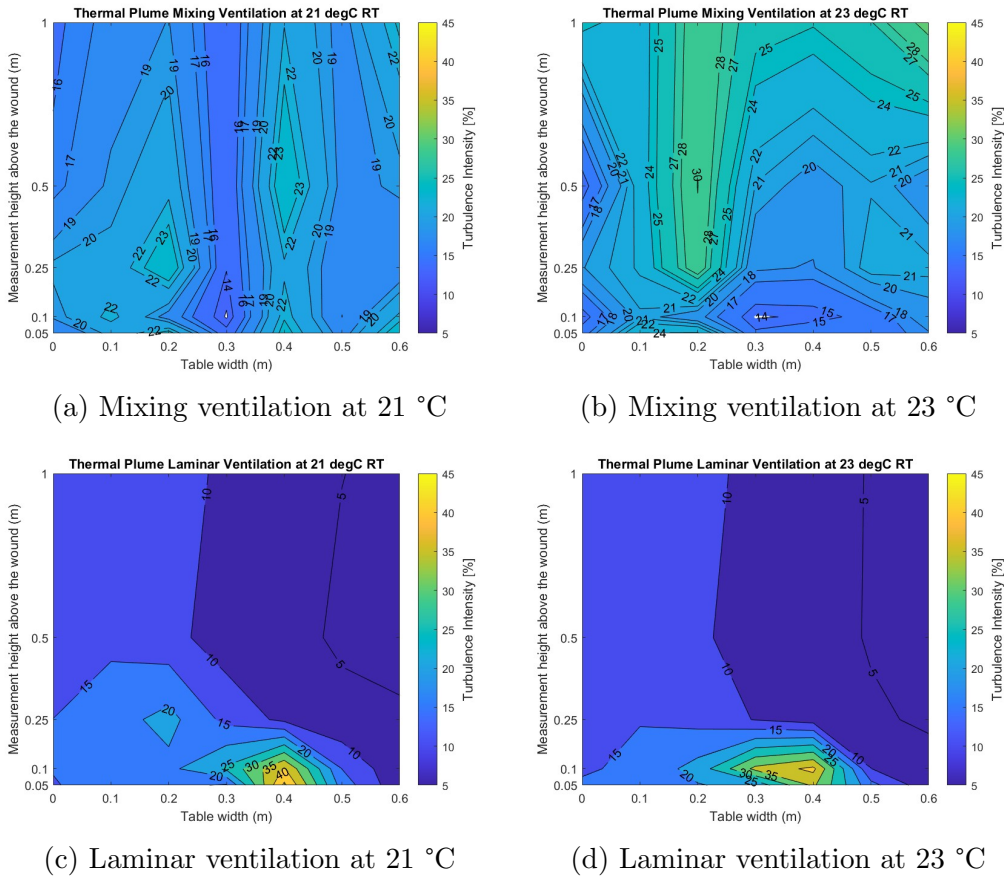
Figure 5.8: Turbulence intensity profile of the patient's thermal plume.

The centre of the thermal plume, in Figure 5.8a just above the wound, illustrates a vertical chimney where the TI is lowest. This stands for the laminar flow in the TP and it is encircled by areas with higher TI which exemplifies the interaction between the thermal plume and surrounding air. This chart can also provide an idea of the height of the thermal plume and as seen in case A, it is higher than 100 cm.

A comparable trend can be observed in Figure 5.8b, however, the centre of

the TP is further shifted to the right and as the TP does not reach the highest measured height, the encircled areas with a greater TI can be detected.

The remaining two cases show a disparate tendency since the topmost TI is found at 5 cm for Figure 5.8c and at 10 cm above the wound for Figure 5.8d. This is due to the fact that the most turbulent point would be where the TP meets the supply airflow. Additionally, case D comprises a larger area of higher TI than case C. The reasoning behind this lies in the fact that the TP has a lower buoyancy force and tends to widen the TP in contrast to case C. Moreover, the supply air for case C is denser as the temperature is lower than for case D, which signifies that the unidirectional air is heavier and therefore can suppress the thermal plume closer to the wound.

5.5 Calculations

Theoretical calculations, including room average velocity for the MV scenarios, were made to corroborate the experimental results and be able to obtain a more exhaustive understanding. Furthermore, the calculations to convert the speed into velocity were also displayed to show the importance of making the correction.

5.5.1 Average room velocity

Table 5.1 shows the input data and values of the average room velocity calculations using the equations in section 3.2. Calculations of the same MV room under two different temperatures were performed and compared in order to understand what aspects influence the ventilation in the room.

For 21 °C air room temperature, the aspect that most appear to affect the air movement is the supply inlet followed by the exhaust fan. Gravity and the mannequin's heat play an almost insignificant part in comparison. The average room velocity for the mentioned temperature conditions is calculated to be 0.1084 m/s. From Figure 5.6a it can be seen that a mean velocity of 0.11 m/s surrounds a zone with higher velocities as it gets closer

Table 5.1: Calculation of average room velocity in MV OR at 21 °C and 23 °C using equations in section 3.2.

Design Setup	Units	21 °C	23 °C
	Room		
	Height [m]	2.9	2.9
	Length [m]	7.9	7.9
	Width [m]	7.15	7.15
	Heat Source		
	Φ_h [W]	60	60
Input Data	Δh [m]	1.9	1.9
	h_o [m]	0.418	0.418
	Airflow		
	q_s $[m^3/s]$	1.02	1.02
	q_e $[m^3/s]$	0.89	0.9
	u_o [m/s]	5	5
	T_s [°C]	18.9	23.3
	T_r [°C]	21	23
	ρ_s $[kg/m^3]$	1.18	1.16
	ρ_r $[kg/m^3]$	1.17	1.16
	Kinetic Energy		
	e_i [W]	15.0327	14.8597
	e_o [W]	13.1346	13.1365
Calculations of parameters	e_h [W]	0.0145	0.0144
	e_g [W]	0.2465	0.0524
	Room		
	V_r $[m^3]$	163.8	163.8
	A_s $[m^2]$	200.26	200.26
Average Room velocity	u_r $[m/s]$	0.1084	0.1130

to the wound. This zone displays the velocity profile of the TP while the velocity surrounding it is assumed to be room velocity. The calculated room average velocity corroborates this hypothesis since the numbers align. This calculation also verifies the existence of a fully mixed room in the OR for case A.

Regarding case B, the average room temperature is slightly greater than for case A, and unlike the previous figure, in Figure 5.6b one cannot distinguish the interaction between the TP and room air easily. The calculated room

velocity is 0.1130 m/s which from the measured velocities it does not correspond to the surrounding velocity. The low velocity and high TI seen in this case could suggest a stagnation area above the wound becoming a risk for the patient. Since the average room velocity calculation assumes a fully mixed room, stagnation areas or velocities are not considered, hence, showing different values.

5.5.2   Speed correction for anemometers

Table 5.2 indicates the values of the measured speed vs the converted velocity for the same points. The columns stand for the position of the anemometer and it can be better understood in Figure 4.14. Every speed value is greater than the velocity ones given the fact that the former does not take direction into account. The wrong assumption of using speed instead of velocity could lead to errors as defined in the 4th row. The error values are different for different points since this depends on the magnitude of turbulence intensity.

Table 5.2: Speed conversion onto velocity of anemometers from MV 23 °C at 10 cm above the wound.

	P1	**P2**	**P3**	**P4**	**P5**	**P6**	**P7**
Speed	0.1237	0.1196	0.1204	0.1300	0.1370	0.1422	0.1415
Velocity	0.1210	0.1148	0.1159	0.1270	0.1337	0.1381	0.1369
Error [%]	2.1426	3.9955	3.7049	2.2622	2.3687	2.8800	3.2901

Chapter 6

Discussion

The ventilation system in an operating room is crucial for the impediment to the spreading of microorganisms and particles. The thermal plume takes an important role in the airflow of the microenvironment and studies have highlighted that an adequate ventilation system should be placed to counteract the possible aftereffect of the thermal plume.

6.1 Indoor environment parameters

The room temperatures inside the ORs were established to be 21 and 23 °C to study the influence of the thermal plume. However, after asking the staff at St. Olavs Hospital which temperature was the most common to use during surgeries, the answer given was 25 °C since this reduces the risk of hypothermia in patients. Checking Table 2.1 one can observe that these temperatures are within the ranges of European standards.

Regarding humidity, the highest value obtained was during the measurements of case B, figuring 14.9 %. At first, it was expected to obtain a lower RH value than case A, however, in both OR a similar trend can be seen. Since the measurements were taken in the same OR as another ongoing study that required 5 people to perform a mock-up surgery, the values of RH are quite different from expected. Case A was measured before the mock-up surgery, showing a low RH value of 7.8 % while Case B was measured straight after the

4-hour mock-up surgery. Human breath is known to produce humidity and so it is not surprising that the value of relative humidity increased after the mock-up surgeries. Comparing the value to the standards, the RH does not reach the minimum requirement. This should be notified to the hospital to make improvements such as installing humidifiers in their ventilation systems. The remaining parameters: supply velocity, airflow, and pressure difference are achieved and considered adequate.

6.2   Thermal plume velocities

For the mixing ventilation, the velocities were highest closer to the wound, and as the plume dissipated and blended with the room air, the velocities decelerated. For the 23 °C case, the air densities between the room and the TP became similar and the mixing happened faster in comparison to the 21 °C scenario. Overall, the velocities for the lower air temperature have a faster thermal plume. A study done by Chongqing University also found that the velocities for a lower temperature room resulted in a higher TP velocity and as the temperature increased, the velocities became slower [91]. For the LAF scenarios, the charts show the highest velocity farthest away from the wound due to the laminar air supply. As it gets closer to the wound, the velocities decrease obtaining the lowest value at 5 cm and 10 cm for the 21 °C and 23 °C scenarios respectively. These points represent the interaction between the upward thermal plume and the downward unidirectional flow.

6.3   Thermal plume temperatures

The maximum temperatures for the lowest temperature case are 23.4 °C for MV and 22.6 °C for LAF. The reason behind not obtaining the same temperatures even though the mannequin's properties were the same, is that the thermal plume for the LAF was suppressed at 5 cm as explained previously, and thus not able to reach as high temperatures. A similar trend appears to happen for case B which reaches a maximum temperature of 25 °C while

case D achieves 24.5 °C. When comparing both temperatures, the TP with 21 °C appears to have a narrower plume while the remaining scenario tends to have a shorter plume with a wider plume base closer to the wound.

A second temperature peak on the right side of the operating table can be observed in every case. This has been thought to be due to a gap in the tape surrounding the wound as shown in Figure 6.1. The heat stored under the blanket is emitted through the gap, producing the second peak.
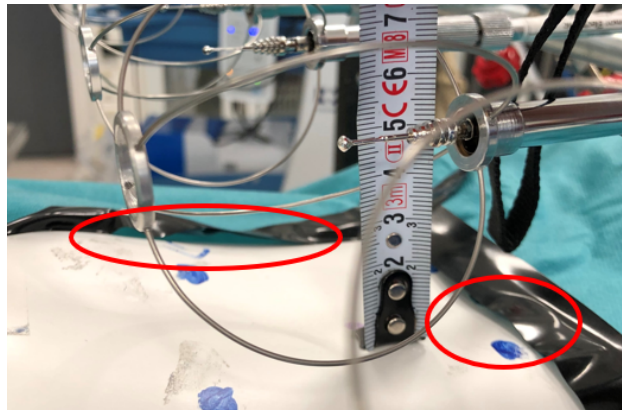
Figure 6.1: Illustration of the unattached tape.

6.4 Thermal plume turbulence intensities

Turbulence intensities are useful to determine the existence of eddies or fluctuations in the air. The mixing ventilation scenario with 21 °C demonstrates a uniform vertical plume that reaches at least 100 cm above the wound with eddies forming on the boundary of the TP. This tendency is also seen in the same room at a higher temperature, howbeit the plume is shifted to the right due to a lower temperature difference. In addition, case B happens to form eddies with greater value over a wider area, signifying its capability to mix easily with the room air. As for the LAF room, the turbulence intensities are truly similar except for the interaction between the thermal plume and laminar air meeting at different heights as already mentioned. A high TI for the LAF cases does not represent the formation of eddies but the interaction between the unidirectional flow and TP. For both cases, the laminar flow

predominates the microenvironment zone above 25 cm. The shape of the TP being narrower for the 21 ℃ cases and widen at the bottom for the 23 ℃ scenarios is also illustrated by the TI.

6.5   Reduction of SSI

Previous studies have stated that having a higher thermal plume in the mixing ventilation contributes to lowering the risk of SSI as it protects the wound from incoming particles. The ability of the plume to transport particles upwards depends on the heat flux [91]. Equation 6.1 represents Newton's cooling law for convective heat transfer where h is the convective heat transfer coefficient $[W/m^2]$, t_s is the temperature of the mannequin's surface [K], and t_f the air temperature [K].

$$q_f = h(t_s - t_f) \tag{6.1}$$

Based on Newton's law, the higher the temperature difference between the patient's temperature and room air, the greater the ability of the plume to diffuse the particles upwards. As for the LAF OR, it was stated in the literature section that the higher the thermal plume is, the greater the risk of indirect infection.

Particles tend to follow the air streams in a room hence the understanding of the air distribution is important to locate BCP. Eddies are circular currents that have the ability to transport particles to one location and trap them, resulting in high BCP concentrations [38]. Case B is composed of a big eddy with high-velocity fluctuations close to the wound, having the highest chance of SSI out of the remaining cases. As for the LAF OR, it was stated in the literature section that the higher the thermal plume is, the greater the risk of indirect infection. Therefore, from an SSI preventative point of view, the best scenarios for both operating rooms are performing surgeries at 21 ℃ room temperature.

6.6 Theoretical calculations

The average room velocity calculations for the turbulent mixing ventilation and the measurements in the same room resulted being very similar for case A. This indicates that the operating room at St. Olavs Hospital at this room temperature reaches a fully mixed air distribution, having the potential to dilute the pollutants at any point in the room. Furthermore, the equations were proven to work for the OR at the hospital, hence they can be used for future research. Regarding case B, further investigations should be made to determine the existence of stagnation zones which could become a potential risk for the patient.

For the speed correction equations, the results confirm the theory of having higher speed values than velocity. In addition, calculations of the error percentage of using the speed as velocity were portrayed in the result section, suggesting that if the correction is neglected, the results would have an inaccuracy of 3 %.

Asymmetrical thermal plume calculations were also studied to understand the physics behind it and provide stronger arguments for the result's interpretations.

Since the amount of BCP and its movement around the room is crucial to determine the risk of SSI, equations of particle motion following the air streams, as well as particle tracking methods and particle deposition, were provided for the sole purpose of understanding the phenomenon. Unfortunately, due to a lack of data, these numerical calculations were not possible to determine, however, they could be used in future research.

6.7   Limitations

Previous studies establish that performing the measurements with a breathing mannequin results in a wider plume cross-section in comparison to a no-breathing one [60]. Not having the correct thermal plume's shape could lead to incorrect velocities which in themselves signifies an incorrect SSI risk estimation for the ORs.

Regarding the analysis of the results for the anemometers data, an interpolation function was used and due to distances not being equidistant, errors due to data uncertainty are present.

Concerning the theoretical calculations for the average room velocity, some aspects of Equation 3.2, such as infiltration and exfiltration, were assumed non-existent as ORs ought to be airtight to reach pressure differences. The mentioned equation does take into account the position of the supply diffusers and instead, one bigger diffuser was assumed. In addition, the calculated surface temperatures were presumed to be constant and the ventilation system achieved a fully mixed room.

A female mannequin that was 1.7 m tall was utilised due to its lightest weight and easy transportation to the hospital. Since the thermal plume is determined by the shape, choosing another mannequin with different gender and/or size might have affected the results.

6.8   Further work

The results show that the thermal plume for both systems protects the wound best at 21 °C since for mixing ventilation it dominates the critical zone reaching higher heights and for laminar airflow, the thermal plume is suppressed closer to the wound. It could be interesting to repeat the measurements with particle counting or particle image velocimetry (PIV) to confirm this hypothesis.

Another interesting concept to further investigate is the asymmetrical shape of the plume over the patient to explore the cross-sectional area from section 3.3 and understand how this can influence the risk of SSI.

Additional further work that can contribute to understanding the airflow distribution in the room, ergo the particle movement, is to simulate the two study cases with computational fluid dynamic (CFD) using the given equations.

To determine if there is a balance between low microbial contamination and low energy consumption in St. Olavs Hospital, it could be interesting to study the environmental quality indicators to determine the requisites and decide on possible beneficial changes.

Chapter 7

Conclusion

This study has highlighted the influence of the patient's thermal plume during surgery and how it could contribute to the reduction of SSI in the critical zone. It also displayed the thermal plume difference between the laminar airflow and turbulent mixing ventilation surgery rooms and the effect that the room temperature has on a lying thermal plume. The conclusions are summarised as follows:

- Thermal plumes in turbulent mixing operating rooms appear to reach higher velocity values at lower air room temperatures.

- Maximum temperatures for the LAF scenarios are not the same as for MV since the unidirectional flow suppresses the thermal plume.

- The turbulence intensity for case A shows a unidirectional flow above the wound and the formation of eddies on the boundary.

- The thermal plume for case B diffuses more easily than case A due to a lower density difference between the room air and the patient's thermal plume, resulting in bigger and more turbulent eddies.

- The height of the thermal plume for LAF increases with the room temperature.

- After 25 cm above the wound, the unidirectional flow dominates the critical zone for both 21 and 23 °C.

- From an infection-preventative standpoint, surgeries performed at 21 ℃ have a lower SSI risk than at 23 ℃ for both LAF and MV systems.

- The parameters measured in the operating rooms seemed to be within standard regulations except for the relative humidity. The maximum value of 14.9 % during case B was still below the suggested one by the standards.

Bibliography

[1] O. M. Lidwell, E. J. Lowbury, W. Whyte, R. Blowers, S. J. Stanley, and D. Lowe, "Effect of ultraclean air in operating rooms on deep sepsis in the joint after total hip or knee replacement: A randomised study.," *BMJ*, vol. 285, no. 6334, pp. 10–14, 1982, ISSN: 0007-1447. DOI: 10.1136/bmj.285.6334.10. eprint: https://www.bmj.com/content/285/6334/10.full.pdf. [Online]. Available: https://www.bmj.com/content/285/6334/10.

[2] J. Liston and A. Bayles, "Surgical site infections," *Surgery (Oxford)*, vol. 41, no. 2, pp. 65–70, 2023, ISSN: 0263-9319. DOI: https://doi.org/10.1016/j.mpsur.2022.11.009. [Online]. Available: https://www.sciencedirect.com/science/article/pii/S0263931922002411.

[3] S. Sadrizadeh, A. Tammelin, P. Ekolind, and S. Holmberg, "Influence of staff number and internal constellation on surgical site infection in an operating room," *Particuology*, vol. 13, pp. 42–51, 2014, ISSN: 1674-2001. DOI: https://doi.org/10.1016/j.partic.2013.10.006. [Online]. Available: https://www.sciencedirect.com/science/article/pii/S167420011300223X.

[4] S. S. Awad, "Adherence to surgical care improvement project measures and post-operative surgical site infections," *Surgical Infections*, vol. 13, no. 4, pp. 234–237, 2012, PMID: 22913334. DOI: 10.1089/sur.2012.131. eprint: https://doi.org/10.1089/sur.2012.131. [Online]. Available: https://doi.org/10.1089/sur.2012.131.

[5] M. Alsved, A. Civilis, P. Ekolind, *et al.*, "Temperature-controlled airflow ventilation in operating rooms compared with laminar airflow and

turbulent mixed airflow," *Journal of Hospital Infection*, vol. 98, no. 2, pp. 181–190, 2018, ISSN: 0195-6701. DOI: https://doi.org/10.1016/j.jhin.2017.10.013. [Online]. Available: https://www.sciencedirect.com/science/article/pii/S0195670117305790.

[6] S. Scaltriti, S. Cencetti, S. Rovesti, I. Marchesi, A. Bargellini, and P. Borella, "Risk factors for particulate and microbial contamination of air in operating theatres," *Journal of Hospital Infection*, vol. 66, no. 4, pp. 320–326, 2007, ISSN: 0195-6701. DOI: https://doi.org/10.1016/j.jhin.2007.05.019. [Online]. Available: https://www.sciencedirect.com/science/article/pii/S0195670107001843.

[7] J. A. Wagner, D. G. Greeley, T. C. Gormley, and T. A. Markel, "Comparison of operating room air distribution systems using the environmental quality indicator method of dynamic simulated surgical procedures," *American Journal of Infection Control*, vol. 47, no. 1, e1–e6, 2019, ISSN: 0196-6553. DOI: https://doi.org/10.1016/j.ajic.2018.07.020. [Online]. Available: https://www.sciencedirect.com/science/article/pii/S0196655318308095.

[8] S. Iudicello and A. Fadda, "A road map to a comprehensive regulation on ventilation technology for operating rooms," *Infection Control amp; Hospital Epidemiology*, vol. 34, no. 8, pp. 858–860, 2013. DOI: 10.1086/671261.

[9] Z. Liu, D. Yin, L. Hu, J. He, and G. Cao, "Bacteria-carrying particles diffusion in the operating room due to the interaction between human thermal plume and ventilation systems: An experimental-numerical simulation study," *Energy and Buildings*, vol. 270, p. 112 277, 2022, ISSN: 0378-7788. DOI: https://doi.org/10.1016/j.enbuild.2022.112277. [Online]. Available: https://www.sciencedirect.com/science/article/pii/S0378778822004480.

[10] Z. Liu, D. Yin, Y. Niu, G. Cao, H. Liu, and L. Wang, "Effect of human thermal plume and ventilation interaction on bacteria-carrying particles diffusion in operating room microenvironment," *Energy and Buildings*, vol. 254, p. 111 573, 2022, ISSN: 0378-7788. DOI: https:

`//doi.org/10.1016/j.enbuild.2021.111573`. [Online]. Available: `https://www.sciencedirect.com/science/article/pii/S0378778821008574`.

[11] P. Dancă, A. Jamin, I. Nastase, B. Janssens, W. Bosschaerts, and C. Coşoiu, "Experimental and numerical study of the flow dynamics and thermal behavior inside a car cabin: Innovative air diffusers and human body plumes interactions," *Energy Reports*, vol. 8, pp. 992–1002, 2022, Technologies and Materials for Renewable Energy, Environment and Sustainability, ISSN: 2352-4847. DOI: `https://doi.org/10.1016/j.egyr.2022.07.133`. [Online]. Available: `https://www.sciencedirect.com/science/article/pii/S2352484722014007`.

[12] S. Iudicello and A. Fadda, "A road map to a comprehensive regulation on ventilation technology for operating rooms," *Infection Control & Hospital Epidemiology*, vol. 34, no. 8, pp. 858–860, 2013. DOI: `10.1086/671261`.

[13] J. M. and K. W. S. N. M. R. B. J. S. M.-J. R., "Current evidence for the use of laminar flow in reducing infection rates in total joint arthroplasty," *The open orthopaedics journal*, vol. 9, pp. 495–498, 2015. DOI: `https://doi.org/10.2174/1874325001509010495`.

[14] A. C. D'Alicandro, N. Massarotti, and A. Mauro, "Aerosol hazards in operating rooms: A review of numerical and experimental studies," *Journal of Aerosol Science*, vol. 158, p. 105 823, 2021, ISSN: 0021-8502. DOI: `https://doi.org/10.1016/j.jaerosci.2021.105823`. [Online]. Available: `https://www.sciencedirect.com/science/article/pii/S0021850221005541`.

[15] F. S, T. M, H. T, *et al.*, "Reduction of airborne bacterial burden in the or by installation of unidirectional displacement airflow (udf) systems.," *Medical science monitor : international medical journal of experimental and clinical research*, vol. 21, pp. 2367–2374, 2015. DOI: `https://doi.org/10.12659/MSM.894251`.

[16] G. Cao, I. Kvammen, T. A. S. Hatten, *et al.*, "Experimental measurements of surgical microenvironments in two operating rooms with laminar airflow and mixing ventilation systems," *Energy and Built Environment*, vol. 2, no. 2, pp. 149–156, 2021, ISSN: 2666-1233. DOI: https://doi.org/10.1016/j.enbenv.2020.08.003. [Online]. Available: https://www.sciencedirect.com/science/article/pii/S2666123320300854.

[17] M. Fan. "Evaluation on the suitability of different ventilation strategies for operating rooms at st. olavs hospital." (), [Online]. Available: https://ntnuopen.ntnu.no/ntnu-xmlui/bitstream/handle/11250/2621749/no.ntnu:inspera:2526673.pdf?sequence=1. (accessed: 14.11.2022).

[18] K. Xue, G. Cao, M. Liu, *et al.*, "Experimental study on the effect of exhaust airflows on the surgical environment in an operating room with mixing ventilation," *Journal of Building Engineering*, vol. 32, p. 101837, 2020, ISSN: 2352-7102. DOI: https://doi.org/10.1016/j.jobe.2020.101837. [Online]. Available: https://www.sciencedirect.com/science/article/pii/S2352710220334707.

[19] A. Miller, M. Henry, and B. Brause, "1 - prevention of joint infections," in *Management of Periprosthetic Joint Infections (PJIs)*, J. C. Arts and J. Geurts, Eds., Woodhead Publishing, 2017, pp. 3–23, ISBN: 978-0-08-100205-6. DOI: https://doi.org/10.1016/B978-0-08-100205-6.00001-X. [Online]. Available: https://www.sciencedirect.com/science/article/pii/B978008100205600001X.

[20] A. Erichsen Andersson, M. Petzold, I. Bergh, J. Karlsson, B. I. Eriksson, and K. Nilsson, "Comparison between mixed and laminar airflow systems in operating rooms and the influence of human factors: Experiences from a swedish orthopedic center," *American Journal of Infection Control*, vol. 42, no. 6, pp. 665–669, 2014, ISSN: 0196-6553. DOI: https://doi.org/10.1016/j.ajic.2014.02.001. [Online]. Available: https://www.sciencedirect.com/science/article/pii/S019665531400087X.

[21] M. Diab-Elschahawi, J. Berger, A. Blacky, *et al.*, "Impact of different-sized laminar air flow versus no laminar air flow on bacterial counts in the operating room during orthopedic surgery," *American Journal of Infection Control*, vol. 39, no. 7, e25–e29, 2011, ISSN: 0196-6553. DOI: https://doi.org/10.1016/j.ajic.2010.10.035. [Online]. Available: https://www.sciencedirect.com/science/article/pii/S0196655311000575.

[22] P. Bischoff, N. Z. Kubilay, B. Allegranzi, M. Egger, and P. Gastmeier, "Effect of laminar airflow ventilation on surgical site infections: A systematic review and meta-analysis," *The Lancet Infectious Diseases*, vol. 17, no. 5, pp. 553–561, 2017, ISSN: 1473-3099. DOI: https://doi.org/10.1016/S1473-3099(17)30059-2. [Online]. Available: https://www.sciencedirect.com/science/article/pii/S1473309917300592.

[23] G. Cao, A. M. Nilssen, Z. Cheng, L.-I. Stenstad, A. Radtke, and J. G. Skogås, "Laminar airflow and mixing ventilation: Which is better for operating room airflow distribution near an orthopedic surgical patient?" *American Journal of Infection Control*, vol. 47, no. 7, pp. 737–743, 2019, ISSN: 0196-6553. DOI: https://doi.org/10.1016/j.ajic.2018.11.023. [Online]. Available: https://www.sciencedirect.com/science/article/pii/S0196655318311441.

[24] S. Sun, J. Li, and J. Han, "How human thermal plume influences near-human transport of respiratory droplets and airborne particles," *Environ Chem Lett*, vol. 19, pp. 1971–1982, 2021. DOI: https://doi.org/10.1007/s10311-020-01178-4.

[25] B. A. Craven and G. S. Settles, "A computational and experimental investigation of the human thermal plume," *ASME. J. Fluids Eng.*, vol. 128(6), pp. 1261–1258, 2006. DOI: https://doi.org/10.1115/1.2353274.

[26] L. Tacutu, F. Bode, I. Năstase, C. Croitoru, and A. Dogeanu, "Experimental and numerical study on the thermal plumes of a standing and lying human in an operating room," *Science and Technology for*

the Built Environment, vol. 28, no. 1, pp. 2–20, 2022. DOI: 10.1080/23744731.2021.1963133. [Online]. Available: https://doi.org/10.1080/23744731.2021.1963133.

[27] A. Hambraeus, "Aerobiology in the operating roomâ€"a review," *Journal of Hospital Infection*, vol. 11, pp. 68–76, 1988, 1st International Conference of the Hospital Infection Society, ISSN: 0195-6701. DOI: https://doi.org/10.1016/0195-6701(88)90169-7. [Online]. Available: https://www.sciencedirect.com/science/article/pii/0195670188901697.

[28] D. Hansen, C. Krabs, D. Benner, A. Brauksiepe, and W. Popp, "Laminar air flow provides high air quality in the operating field even during real operating conditions, but personal protection seems to be necessary in operations with tissue combustion," *International Journal of Hygiene and Environmental Health*, vol. 208, no. 6, pp. 455–460, 2005, ISSN: 1438-4639. DOI: https://doi.org/10.1016/j.ijheh.2005.08.008. [Online]. Available: https://www.sciencedirect.com/science/article/pii/S1438463905001148.

[29] F. Memarzadeh and A. P. Manning, "Comparison of operating room ventilation systems in the protection of the surgical site," *ASHRAE Transactions*, vol. 108, pp. 3–15, 2002. [Online]. Available: https://www.proquest.com/docview/192532805?pq-origsite=gscholar&fromopenview=true.

[30] C. A. Mackintosh, O. M. Lidwell, A. G. Towers, and R. R. Marples, "The dimensions of skin fragments dispersed into the air during activity," *Journal of Hygiene*, vol. 81, no. 3, pp. 471–480, 1978. DOI: 10.1017/S0022172400025341.

[31] W. Noparat, K. Siripanichakorn, C. Tribuddharat, and S. Danchaivijitr, "Persistence of antimicrobial effect of antiseptics in surgical hand hygiene regimens," *Journal of the Medical Association of Thailand = Chotmaihet thangphaet*, vol. 88, no. 10, pp. 177–182, 2005. [Online]. Available: https://www.thaiscience.info/journals/Article/JMAT/10778496.pdf.

[32] N. J. Mitchell, D. S. Evans, and A. Kerr, "Reduction of skin bacteria in theatre air with comfortable, non-woven disposable clothing for operating-theatre staff.," *British Medical Journal*, vol. 1, no. 6114, pp. 696–698, 1978. DOI: https://doi.org/10.1136/bmj.1.6114.696.

[33] N. Mitchell and D. Gamble, "Clothing design for operating-room personnel," *The Lancet*, vol. 304, no. 7889, pp. 1133–1136, 1974, Originally published as Volume 2, Issue 7889, ISSN: 0140-6736. DOI: https://doi.org/10.1016/S0140-6736(74)90886-1. [Online]. Available: https://www.sciencedirect.com/science/article/pii/S0140673674908861.

[34] Z. Ai, C. M. Mak, N. Gao, and J. Niu, "Tracer gas is a suitable surrogate of exhaled droplet nuclei for studying airborne transmission in the built environment.," *Building Simulation*, vol. 13, pp. 489–496, 2020. DOI: https://doi.org/10.1007/s12273-020-0614-5. [Online]. Available: https://link.springer.com/article/10.1007/s12273-020-0614-5#citeas.

[35] T. Chow and X. Yang, "Ventilation performance in operating theatres against airborne infection: Review of research activities and practical guidance," *Journal of Hospital Infection*, vol. 56, no. 2, pp. 85–92, 2004, ISSN: 0195-6701. DOI: https://doi.org/10.1016/j.jhin.2003.09.020. [Online]. Available: https://www.sciencedirect.com/science/article/pii/S0195670103003979.

[36] Z. Liu, D. Yin, Y. Niu, G. Cao, H. Liu, and L. Wang, "Effect of human thermal plume and ventilation interaction on bacteria-carrying particles diffusion in operating room microenvironment," *Energy and Buildings*, vol. 254, p. 111 573, 2022, ISSN: 0378-7788. DOI: https://doi.org/10.1016/j.enbuild.2021.111573. [Online]. Available: https://www.sciencedirect.com/science/article/pii/S0378778821008574.

[37] C. Yang, X. Yang, and B. Zhao, "The ventilation needed to control thermal plume and particle dispersion from manikins in a unidirectional ventilated protective isolation room," *Building Simulation*, vol. 8,

pp. 551–565, 2015. DOI: https://doi.org/10.1007/s12273-014-0227-6.

[38] Z. Liu, H. Liu, H. Yin, R. Rong, G. Cao, and Q. Deng, "Prevention of surgical site infection under different ventilation systems in operating room environment," *Frontiers of Environmental Science & Engineering volume*, vol. 15, no. 36, 2021. DOI: https://doi.org/10.1007/s11783-020-1327-9.

[39] B. Koelblen and A. Bogdan, "Impact of clothing, breathing and body posture on the shaping of a thermal plume above a human," *International Journal of Ventilation*, vol. 13, no. 4, pp. 397–410, 2015. DOI: 10.1080/14733315.2015.11684063. eprint: https://doi.org/10.1080/14733315.2015.11684063. [Online]. Available: https://doi.org/10.1080/14733315.2015.11684063.

[40] D. Zukowska, Z. Popiolek, and A. Melikov, "Determination of the integral characteristics of an asymmetrical thermal plume from air speed/velocity and temperature measurements," *Experimental Thermal and Fluid Science*, vol. 34, no. 8, pp. 1205–1216, 2010, ISSN: 0894-1777. DOI: https://doi.org/10.1016/j.expthermflusci.2010.04.009. [Online]. Available: https://www.sciencedirect.com/science/article/pii/S0894177710001019.

[41] D. Etheridge and M. Sandberg, *BUILDING VENTILATION, Theory and measurement*. John Wiley and sons (Chichester), 1996.

[42] A. Bouzinaoui, R. Devienne, and J. R. Fontaine, "An experimental study of the thermal plume developed above a finite cylindrical heat source to validate the point source model," *Experimental Thermal and Fluid Science*, vol. 31, no. 7, pp. 649–659, 2007, ISSN: 0894-1777. DOI: https://doi.org/10.1016/j.expthermflusci.2006.06.010. [Online]. Available: https://www.sciencedirect.com/science/article/pii/S0894177706001087.

[43] T. Gormley, T. A. Markel, H. W. Jones, *et al.*, "Methodology for analyzing environmental quality indicators in a dynamic operating room

environment," *American Journal of Infection Control*, vol. 45, no. 4, pp. 354–359, 2017, ISSN: 0196-6553. DOI: https://doi.org/10.1016/j.ajic.2016.11.001. [Online]. Available: https://www.sciencedirect.com/science/article/pii/S0196655316310069.

[44] A. González-Gil, J. López-González, M. Fernández, P. Eguía, A. Erkoreka, and E. Granada, "Thermal energy demand and potential energy savings in a spanish surgical suite through calibrated simulations," *Energy and Buildings*, vol. 174, pp. 513–526, 2018, ISSN: 0378-7788. DOI: https://doi.org/10.1016/j.enbuild.2018.06.059. [Online]. Available: https://www.sciencedirect.com/science/article/pii/S0378778818305619.

[45] ASHRAE, Standard 170-2017, "Ventilation of health care facilities," 2017.

[46] A. G. Constantinos A. Balaras Elena Dascalaki, "Hvac and indoor thermal conditions in hospital operating rooms," *Energy and Buildings*, vol. 39, no. 4, pp. 454–470, 2007, ISSN: 0378-7788. DOI: https://doi.org/10.1016/j.enbuild.2006.09.004. [Online]. Available: https://www.sciencedirect.com/science/article/pii/S0378778806002209.

[47] NHS England and NHS Improvement, *D.o. Health, HTM 01-03 Health Technical Memorandum 03-01: Specialised ventilation for healthcare premises. Part A - Design and installation.* TSO (The Stationery Office), 2021.

[48] Association Française de Normalisation, "Afnor nf s 90-351 établissement de santé : Salles propres et environnements maîtrisés et apparentés," 1997.

[49] Swedish Institute for Standard, "Sis-ts 39:2012," 2012.

[50] Ministerul Dezvoltării Lucrărilor Publice Și Administrației, "Mlpat indicativ c 253," 1994.

[51] Ente nazionale italiano di unificazione, "Uni cen/ts 16244:2018 venti-
lazione negli ospedali - struttura gerarchica coerente e termini e definizioni
comuni per la normativa relativa alla ventilazione negli ospedali," 2018.

[52] H. Koskela, J. Heikkinen, R. Niemelä, and T. Hautalampi, "Turbu-
lence correction for thermal comfort calculation," *Building and En-
vironment*, vol. 36, no. 2, pp. 247–255, 2001, ISSN: 0360-1323. DOI:
https://doi.org/10.1016/S0360-1323(00)00002-0. [Online].
Available: https://www.sciencedirect.com/science/article/
pii/S0360132300000020.

[53] D. Rim and A. Novoselac, "Transport of particulate and gaseous pol-
lutants in the vicinity of a human body," *Building and Environment*,
vol. 44, no. 9, pp. 1840–1849, 2009, ISSN: 0360-1323. DOI: https:
//doi.org/10.1016/j.buildenv.2008.12.009. [Online]. Avail-
able: https://www.sciencedirect.com/science/article/pii/
S0360132308002989.

[54] Z. Popiolek, F. Jørgensen, A. Melikov, M. Silva, and W. Kierat, "As-
sessment of uncertainty in measurements with low velocity thermal
anemometers," *International Journal of Ventilation*, vol. 6, no. 2, pp. 113–
128, 2007. DOI: 10.1080/14733315.2007.11683771. [Online]. Avail-
able: https://doi.org/10.1080/14733315.2007.11683771.

[55] Z. Popiołek, "Estimation of mean speed and speed standard deviation
from cfd prediction," *architecture civil engineering environment*, 2008.
[Online]. Available: http://delibra.bg.polsl.pl/Content/28195/
BCPS_31789_-_Estimation-of-mean-s_0000.pdf.

[56] H. Koskela, J. Heikkinen, R. Niemelä, and T. Hautalampi, "Turbu-
lence correction for thermal comfort calculation," *Building and En-
vironment*, vol. 36, no. 2, pp. 247–255, 2001, ISSN: 0360-1323. DOI:
https://doi.org/10.1016/S0360-1323(00)00002-0. [Online].
Available: https://www.sciencedirect.com/science/article/
pii/S0360132300000020.

[57] K. Hagström, O. Hakkola, and T. Moilanen, "Room average velocity equation - a tool to improve the design of thermal comfort conditions," *Airbase publication*, vol. 3, pp. 760–764, 2002. [Online]. Available: https://www.irbnet.de/daten/iconda/CIB7284.pdf.

[58] K. Hagström and K. Sirén, "Calculation of the room velocity using kinetic energy balance," *ASHRAE Transactions*, vol. 2, pp. 3–12, 2000. [Online]. Available: https://www.aivc.org/sites/default/files/airbase_12974.pdf.

[59] D. Zukowska, Z. Popiolek, and A. Melikov, "New method for calculation of integral characteristics of thermal plumes," *Indoor Air*, pp. 17–22, 2008. [Online]. Available: https://www.researchgate.net/profile/Daria-Zukowska-Tejsen/publication/349466864_New_method_for_calculation_of_integral_characteristics_of_thermal_plumes/links/60319ed592851c4ed58790d0/New-method-for-calculation-of-integral-characteristics-of-thermal-plumes.pdf.

[60] D. Zukowska, A. Melikov, Z. Popiolek, and J. Spletsteser, "Impact of breathing on the thermal plume above a human body," *Roomvent*, 2011. [Online]. Available: https://www.researchgate.net/profile/Daria-Zukowska-Tejsen/publication/349466871_Impact_of_breathing_on_the_thermal_plume_above_a_human_body/links/6031a0a4a6fdcc37a83f46b6/Impact-of-breathing-on-the-thermal-plume-above-a-human-body.pdf.

[61] A. Bogdan, K. Ogłodziński, and M. Szyłak-Szydłowski, "Analysis of thermal plumes forming over male human subjects," *Journal of Building Engineering*, vol. 45, p. 103 596, 2022, ISSN: 2352-7102. DOI: https://doi.org/10.1016/j.jobe.2021.103596. [Online]. Available: https://www.sciencedirect.com/science/article/pii/S2352710221014546.

[62] H. Rouse, C. S. Yih, and H. W. Humphreys, "Gravitational convection from a boundary source," *Tellus*, vol. 4, no. 3, pp. 201–210, 1952. DOI: 10.3402/tellusa.v4i3.8688. eprint: https://doi.org/10.3402/

tellusa.v4i3.8688. [Online]. Available: https://doi.org/10.3402/tellusa.v4i3.8688.

[63] T. Lin, O. A. Zargar, K.-Y. Lin, *et al.*, "An experimental study of the flow characteristics and velocity fields in an operating room with laminar airflow ventilation," *Journal of Building Engineering*, vol. 29, p. 101 184, 2020, ISSN: 2352-7102. DOI: https://doi.org/10.1016/j.jobe.2020.101184. [Online]. Available: https://www.sciencedirect.com/science/article/pii/S2352710219317358.

[64] D. Rim and A. Novoselac, "Ventilation effectiveness as an indicator of occupant exposure to particles from indoor sources," *Building and Environment*, vol. 45, no. 5, pp. 1214–1224, 2010, ISSN: 0360-1323. DOI: https://doi.org/10.1016/j.buildenv.2009.11.004. [Online]. Available: https://www.sciencedirect.com/science/article/pii/S0360132309003291.

[65] K. Chung, "Three-dimensional analysis of airflow and contaminant particle transport in a partitioned enclosure," *Building and Environment*, vol. 34, no. 1, pp. 7–17, 1998, ISSN: 0360-1323. DOI: https://doi.org/10.1016/S0360-1323(97)00073-5. [Online]. Available: https://www.sciencedirect.com/science/article/pii/S0360132397000735.

[66] J. E. Martin and E. Meiburg, "The accumulation and dispersion of heavy particles in forced two-dimensional mixing layers. i. the fundamental and subharmonic cases," *Physics of Fluids*, vol. 6, pp. 1116–1132, 1994. DOI: https://doi.org/10.1063/1.868283.

[67] V. Yakhot, S. A. Orszag, and S. Thangam, "Development of turbulence models for shear flows by a double expansion technique," *Physics of Fluids A: Fluid Dynamics*, vol. 4, pp. 1510–1520, 1992. DOI: https://doi.org/10.1063/1.858424. [Online]. Available: https://www.sciencedirect.com/science/article/pii/S167420011300223X.

[68] W. C, H. S, and S. S., "Impact of door opening on the risk of surgical site infections in an operating room with mixing ventilation," *Indoor*

and Built Environment, vol. 30, pp. 166–179, 2021. DOI: https://doi.org/10.1177/1420326X19888276.

[69] K. Van Maele and B. Merci, "Application of two buoyancy-modified k–ε turbulence models to different types of buoyant plumes," *Fire Safety Journal*, vol. 41, no. 2, pp. 122–138, 2006, ISSN: 0379-7112. DOI: https://doi.org/10.1016/j.firesaf.2005.11.003. [Online]. Available: https://www.sciencedirect.com/science/article/pii/S0379711205001207.

[70] F. Kuznik, G. Rusaouën, and J. Brau, "Experimental and numerical study of a full scale ventilated enclosure: Comparison of four two equations closure turbulence models," *Building and Environment*, vol. 42, no. 3, pp. 1043–1053, 2007, ISSN: 0360-1323. DOI: https://doi.org/10.1016/j.buildenv.2005.11.024. [Online]. Available: https://www.sciencedirect.com/science/article/pii/S0360132305004841.

[71] Z. Zhang and Q. Chen, "Experimental measurements and numerical simulations of particle transport and distribution in ventilated rooms," *Atmospheric Environment*, vol. 40, no. 18, pp. 3396–3408, 2006, ISSN: 1352-2310. DOI: https://doi.org/10.1016/j.atmosenv.2006.01.014. [Online]. Available: https://www.sciencedirect.com/science/article/pii/S1352231006000768.

[72] S. Sadrizadeh, A. Tammelin, P. Ekolind, and S. Holmberg, "Influence of staff number and internal constellation on surgical site infection in an operating room," *Particuology*, vol. 13, pp. 42–51, 2014, ISSN: 1674-2001. DOI: https://doi.org/10.1016/j.partic.2013.10.006. [Online]. Available: https://www.sciencedirect.com/science/article/pii/S167420011300223X.

[73] S. A. Morsi and A. J. Alexander, "An investigation of particle trajectories in two-phase flow systems," *Journal of Fluid Mechanics*, vol. 55, pp. 193–208, 1972. DOI: https://doi.org/10.1017/S0022112072001806.

[74] E. Hathway, C. Noakes, P. Sleigh, and L. Fletcher, "Cfd simulation of airborne pathogen transport due to human activities," *Building and*

Environment, vol. 46, no. 12, pp. 2500–2511, 2011, ISSN: 0360-1323. DOI: https://doi.org/10.1016/j.buildenv.2011.06.001. [Online]. Available: https://www.sciencedirect.com/science/article/pii/S0360132311001727.

[75] S. Lestinen, S. Kilpeläinen, R. Kosonen, J. Jokisalo, H. Koskela, and A. Melikov, "Flow characteristics in occupied zone – an experimental study with symmetrically located thermal plumes and low-momentum diffuse ceiling air distribution," *Building and Environment*, vol. 128, pp. 77–88, 2018, ISSN: 0360-1323. DOI: https://doi.org/10.1016/j.buildenv.2017.11.020. [Online]. Available: https://www.sciencedirect.com/science/article/pii/S0360132317305279.

[76] A. C. K. Lai and W. W. Nazaroff, "Modeling indoor particle deposition from turbulent flow onto smooth surfaces," *Journal of Aerosol Science*, vol. 31, no. 4, pp. 463–476, 2000, ISSN: 0021-8502. DOI: https://doi.org/10.1016/S0021-8502(99)00536-4. [Online]. Available: https://www.sciencedirect.com/science/article/pii/S0021850299005364.

[77] N. Gao and J. Niu, "Modeling particle dispersion and deposition in indoor environments," *Atmospheric Environment*, vol. 41, no. 18, pp. 3862–3876, 2007, ISSN: 1352-2310. DOI: https://doi.org/10.1016/j.atmosenv.2007.01.016. [Online]. Available: https://www.sciencedirect.com/science/article/pii/S135223100700060X.

[78] B. Zhao and J. Wu, "Modeling particle deposition from fully developed turbulent flow in ventilation duct," *Atmospheric Environment*, vol. 40, no. 3, pp. 457–466, 2006, ISSN: 1352-2310. DOI: https://doi.org/10.1016/j.atmosenv.2005.09.043. [Online]. Available: https://www.sciencedirect.com/science/article/pii/S1352231005008897.

[79] Sensor electronic. "Airdistsys 5000. user's manual." (), [Online]. Available: http://www.sensor-electronic.pl/pdf/KAT_AirDistSys5000.pdf. (accessed: 10.12.2022).

[80] Gemeni data logger. "Tinytag plus 2 tgp-4500 data sheet." (), [Online]. Available: http://gemini2.assets.d3r.com/pdfs/original/3751-tgp-4500.pdf. (accessed: 10.12.2022).

[81] S. Tanabe, E. A. Arens, F. Bauman, H. Zhang, and T. Madsen, "Evaluating thermal environments by using a thermal manikin with controlled skin surface temperature," *ASHRAE*, vol. 100, no. 1, pp. 39–48, 1994. [Online]. Available: https://escholarship.org/uc/item/22k424vp.

[82] G. Cao, M. C. Storås, A. Aganovic, L.-I. Stenstad, and J. G. Skogås, "Do surgeons and surgical facilities disturb the clean air distribution close to a surgical patient in an orthopedic operating room with laminar airflow?" *American Journal of Infection Control*, vol. 46, no. 10, pp. 1115–1122, 2018, ISSN: 0196-6553. DOI: https://doi.org/10.1016/j.ajic.2018.03.019. [Online]. Available: https://www.sciencedirect.com/science/article/pii/S0196655318302128.

[83] Teledyne Flir. "Technical data - gen one." (), [Online]. Available: https://www.flir.com/products/flir-one-gen-3/. (accessed: 08.05.2023).

[84] GAO. "Technical data - gao emt707ctl operating instructions manual." (), [Online]. Available: https://www.manualslib.com/manual/1085339/Gao-Emt707ctl.html?page=10#manual. (accessed: 08.05.2023).

[85] Bosch. "Technical data - ptd 1." (), [Online]. Available: https://www.manua.ls/bosch/ptd-1/manual?p=1. (accessed: 08.05.2023).

[86] Bosch. "Bosch zamo - instructions manual." (), [Online]. Available: https://www.manualslib.com/manual/1103454/Bosch-Zamo.html?page=19#manual. (accessed: 10.05.2023).

[87] Obs Bygg. "Bosch zamo ii laseravstandsmåler." (), [Online]. Available: https://www.obsbygg.no/verktoy-og-tilbehor/elektroverktoy/maleverktoy/2328025. (accessed: 10.05.2023).

[88] RS. "Variable transformers." (), [Online]. Available: https://uk.rs-online.com/web/generalDisplay.html?id=solutions/electronics-variable-transformers-content#:~:text=Variable%5C%20transformers%

5C%20are%5C%20transformers%5C%20that,are%5C%20built%5C%20to%5C%20custom%5C%20specifications.. (accessed: 10.05.2023).

[89] T. Chow, A. Kwan, Z. Lin, and W. Bai, "Conversion of operating theatre from positive to negative pressure environment," *Journal of Hospital Infection*, vol. 64, no. 4, pp. 371–378, 2006, ISSN: 0195-6701. DOI: https://doi.org/10.1016/j.jhin.2006.07.020. [Online]. Available: https://www.sciencedirect.com/science/article/pii/S0195670106003859.

[90] S.J.Leach, "Stratification and mixing of fluids of different densities," *Instn chem. Engrs, Symposium series*, vol. 25, 1968. [Online]. Available: https://www.icheme.org/media/10296/iii-paper-03.pdf.

[91] G. Feng, Y. Bi, Y. Zhang, Y. Cai, and K. Huang, "Study on the motion law of aerosols produced by human respiration under the action of thermal plume of different intensities," *Sustainable Cities and Society*, vol. 54, p. 101 935, 2020, ISSN: 2210-6707. DOI: https://doi.org/10.1016/j.scs.2019.101935. [Online]. Available: https://www.sciencedirect.com/science/article/pii/S2210670719316385.

Chapter A

Measuring instruments

The aim of this section is to provide calibration certificates and accuracy graphs for some of the used measuring instruments.
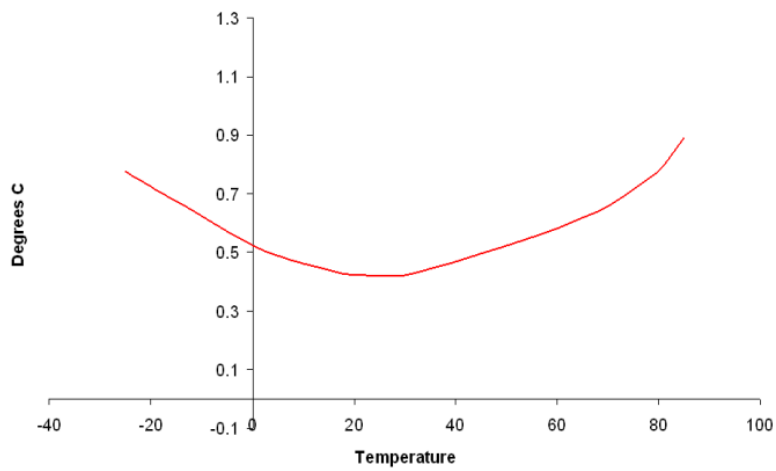

Figure A.1: Image of the temperature accuracy for TinyTag [80].

Q

Test result of Transducer Unit : A 077K105-200 **739**　　　**No: 10**

Anemometer Static Test Result

| Test conditions: | - barometric pressure, Pb [hPa]: | 993.0 |
| | - mean temperature, [°C]: | 20.1 |

Model velocity	Anemo velocity	Anemo velocity corrected *)	Error	Error/ permissible error
V	Vnom	Va	DV=Va-V	DV/DP
[m/s]	[m/s]	[m/s]	[m/s]	[%]
4.78	4.68	4.78	-0.01	-6.1
4.02	3.91	3.99	-0.03	-38.2
3.29	3.22	3.28	0.00	-7.3
2.78	2.72	2.77	-0.01	-11.5
2.39	2.33	2.37	-0.01	-27.3
1.99	1.95	1.99	0.00	6.1
1.60	1.56	1.59	-0.01	-23.1
1.30	1.28	1.30	0.00	5.1
1.010	0.986	1.006	-0.004	-11.5
0.810	0.799	0.815	0.005	15.6
0.608	0.600	0.612	0.004	13.8
0.514	0.505	0.515	0.001	3.6
0.412	0.405	0.413	0.001	3.8
0.306	0.297	0.303	-0.003	-12.3
0.202	0.194	0.198	-0.004	-17.5
0.153	0.145	0.148	-0.005	-22.5
0.099	0.094	0.096	-0.003	-14.0
0.077	0.074	0.075	-0.002	-9.5
0.052	0.048	0.049	-0.003	-14.5

*) Note: The barometric pressure influence on velocity is presented below:

$V_a = V_{nom} * P_{nom}/P_b$, where P_{nom} - standard barometric pressure 1013hPa

CHART OF ERRORS
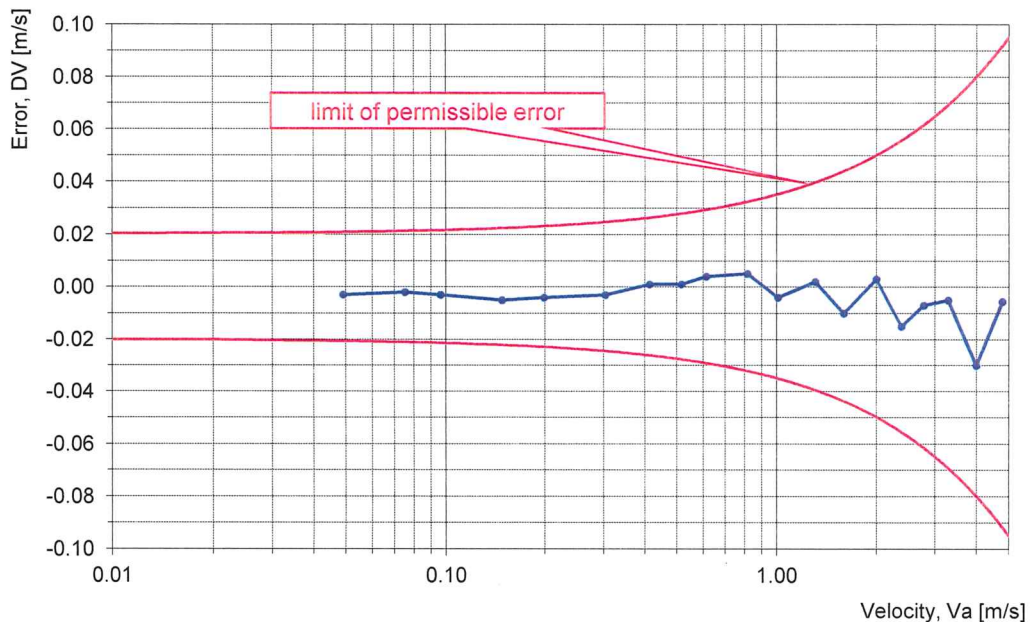
Thermometer test result

Test conditions:	- in air flow above, [m/s]:	0.10
- temp. measured by reference thermometer, [°C]:		20.1
- temp. measured by tested transducer, [°C]:		20.2
Error:　0.1°C		

Chapter B

Matlab script

The Matlab scripts used to analyse the data are shown in this section.

B.1   Script for temperature, velocity and turbulence intensity profiles

```
clear all
clc

filepath5 = "C:\Users\marin\Desktop\Master\4
   semester\21 degC\vel_5_LAF.txt";
filepath10 = "C:\Users\marin\Desktop\Master\4
   semester\21 degC\vel_10_LAF.txt";
filepath25 = "C:\Users\marin\Desktop\Master\4
   semester\21 degC\vel_25_LAF.txt";
filepath50 = "C:\Users\marin\Desktop\Master\4
   semester\21 degC\vel_50_LAF.txt";
filepath100 = "C:\Users\marin\Desktop\Master\4
   semester\21 degC\vel_98_LAF.txt";

[TI5, v5, T5] = f(filepath5);
[TI10, v10, T10] = f(filepath10);
```

```matlab
[TI25, v25, T25] = f(filepath25);
[TI50, v50, T50] = f(filepath50);
[TI100, v100, T100] = f(filepath100);


t=[mean(T5);mean(T10);mean(T25);mean(T50);mean(T100)
   ];
t=t(:,[1 2 3 7 4 5 6]);
v=[v5; v10; v25; v50; v100];
TU=[mean(TI5); mean(TI10); mean(TI25); mean(TI50);
   mean(TI100)];
TU=TU.*100;
TU=TU(:,[1 2 3 7 4 5 6]);


figure
x=linspace(0.1,0.7,7);
y=[0.05 0.10 0.25 0.5 1];
contourf(x,y,t,'ShowText','on')
title('Thermal Plume Laminar Ventilation at 21 degC
   RT')
xticklabels({'0','0.1','0.2','0.3','0.4','0.5','0.6'
   })
yticks([0.05 0.10 0.25 0.5 1])
yticklabels([ 0.05 0.10 0.25 0.5 1])
xlabel('Table width (m)')
ylabel('Measurement height above the wound (m)')
a = colorbar;
ylabel(a,'Air Temperature [degC]','FontSize',11,'
   Rotation', 90);


figure
x=linspace(0.1,0.7,7);
y=[0.05 0.10 0.25 0.5 1];
[c,h]=contourf(x,y,v,12,'ShowText','on');
```

T

```matlab
    h.LevelList=round(h.LevelList,2)
    clabel(c,h)
title('Thermal Plume Laminar Ventilation at 21 degC
    RT')
xticklabels({'0','0.1','0.2','0.3','0.4','0.5','0.6'
    })
yticks([0.05 0.10 0.25 0.5 1])
yticklabels([ 0.05 0.10 0.25 0.5 1])
xlabel('Table width (m)')
ylabel('Measurement height above the wound (m)')
a = colorbar;
ylabel(a,'Air velocity [m/s]','FontSize',11,'
    Rotation', 90);

figure
x=linspace(0.1,0.7,7);
y=[0.05 0.10 0.25 0.5 1];
contourf(x,y,TU,'ShowText','on')
title('Thermal Plume Laminar Ventilation at 21 degC
    RT')
xticklabels({'0','0.1','0.2','0.3','0.4','0.5','0.6'
    })
yticks([0.05 0.10 0.25 0.5 1])
yticklabels([ 0.05 0.10 0.25 0.5 1])
xlabel('Table width (m)')
ylabel('Measurement height above the wound (m)')
a = colorbar;
ylabel(a,'Turbulence Intensity [%]','FontSize',11,'
    Rotation', 90);

function [TI, v, T] = f(filepath)
```

```matlab
opts = delimitedTextImportOptions("NumVariables",
   38);
velLAF = readtable(filepath,opts);
M = table2array(velLAF);
u = M(1:150,1:7);
TI = M(1:150,22:28);
TI = TI/100;
nrows=size(TI,1);
ncols= size(TI,2);
V=ones(nrows,ncols);
for j = 1:nrows
    for i = 1:ncols
        if TI(j,i) > 0.45
            V(j,i)=u(j,i)*(0.173+TI(j,i))/(1.596*(TI
               (j,i))^2+0.226*TI(j,i)+0.308);
        else
            V(j,i)=u(j,i)/(1+(TI(j,i))^2);
        end
    end
end

v=mean(V);
v=v([1 2 3 7 4 5 6]);
T = M(1:150,8:14);
end
```

B.2   Script for indoor parameters in the operating rooms

```matlab
O = table2array(TinytagsExhaust);
TinyE21=O(2:236,2);
HumidityE21=O(2:236,3);
```

```matlab
TinyE23=O(2017:2246,2);
HumidityE23=O(2017:2246,3);

width = 5;
test = func(TinyE21,width);
x=linspace(1,230,9);
figure
yyaxis left
plot(TinyE21)
title('Mixing ventilation System')
xlabel('Duration of mock-up surgery [min]')
ylabel ('Temperature [degC]')
hold on
plot(TinyE23)

yyaxis right
plot(HumidityE21)
plot(HumidityE23)
legend('MV Room Temperature at 21degC', 'MV Room
   temperature at 23degC', 'MV Relative humidity at
   21degC', 'MV Relative humidity at 23degC')
ylabel ('Relative Humidity [%]')
xticks([x])
xticklabels({'0', '5', '10', '15', '20', '25', '30',
    '35'})
xlim([1 230])
```

B.3   Script for airflows in operating rooms

```matlab
TrendileMV = readtable("C:\Users\marin\Desktop\
   Master\4 semester\Trendile_MV.txt", opts);
M = table2array(TrendileMV);
```

W

```matlab
SA21=M(1:41,1);
ST21=M(1:41,3)';
EA21=M(1:41,2)';
ET21=M(1:41,4)';
SA23=M(40:80,1)';
ST23=M(40:80,3)';
EA23=M(40:80,2)';
ET23=M(40:80,4)'
x=linspace(1,41,41);

figure
plot(x,SA21,'b--')
title('Mixing ventilation')
xlabel('Duration of mock-up surgery [min]')
ylabel ('Air flow [m^3/h]')
hold on
plot(x,EA21,'b')
plot(x,SA23,'r--')
plot(x,EA23,'r')
xlim([1 39])
ylim([3100 3800])
legend('Supply air rate 21 degC', 'Exhaust air rate
  MV 21 degC','Supply air rate 23 degC', 'Exhaust
  air rate 23 degC')
```

B.4   Script for average room velocity

```matlab
rho=1.17;
uo=5;
qs=3669/3600;
qe=3229/3600;
esource=60;
```
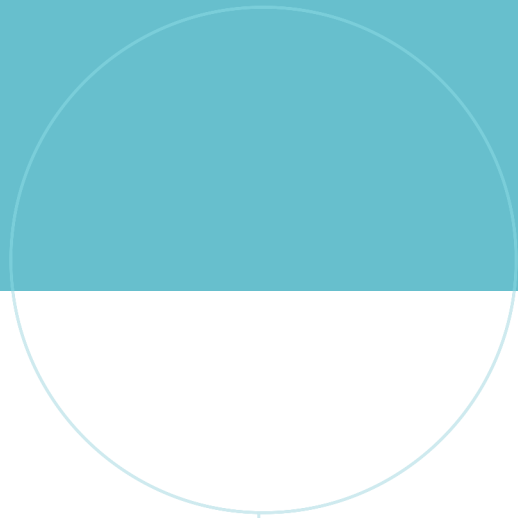
```matlab
L=7.9;
W=7.15;
H=2.9;
dh=1.9;

AN=L*H;
AS=W*H;
F=L*W;
Ts=18.8976;
Tr=21;
ds=1.18;
dr=1.1715;

As=2*AN+2*AS+2*F;
Vr=L*W*H;

eh=0.006*esource^(1/3)*(dh)^(5/3);
eg=9.81*H*qs*(dr-ds);
ei=1/2*rho*uo^2*qs;%Supply
eo=1/2*rho*uo^2*qe;%Exhaust

u_r1=(1.4^(1/2)/ds*(ei+eg+eh-eo)/(0.664*As))^(1/2)*(
    Vr/As)^(1/6)
```